Template-Based Approaches to the Preparation of Amorphous, Nanoporous Silicas

Narayan K. Raman,[†] Mark T. Anderson,[‡] and C. Jeffrey Brinker*[,†,‡]

The UNM/NSF Center for Micro-Engineered Ceramics, University of New Mexico, Albuquerque, New Mexico 87131, and Ceramic Synthesis and Inorganic Chemistry Department, Sandia National Laboratories, Advanced Materials Laboratory, 1001 University Blvd., SE, Albuquerque, New Mexico 87106

Received February 15, 1996[⊗]

This review discusses two classes of organic template-derived amorphous silicas distinguished by the nature of template-matrix interactions and the extent to which subsequent processing dictates the final pore morphology. First we discuss surfactant-templated silicas where the template-matrix interaction is via non-covalent bonding mechanisms and the pore structure is established in the solution stage. We then discuss silicas templated by organic ligands covalently bonded to the siloxane network where subsequent processing strongly influences the final pore structure.

Introduction

The engineering of porosity in common materials such as silica and carbon is emerging as a new area of great technological and scientific interest.[1] Materials with tailor-made pore sizes and shapes are particularly important in applications where molecular recognition is needed, such as shape-selective catalysis, molecular sieving, chemical sensing, and selective adsorption.[2,3] In addition the microporous cavities of zeolites and other engineered porous materials have been used as nanosized reaction vessels[4,5] or hosts in which to assemble semiconductor clusters,[6,7] organic molecules,[8] and even molecular wires[9] in which the dimensional confinement imposed by the framework allows tailoring of optical and electronic properties of the nanocomposite.

One of the earliest synthetic schemes to prepare controlled porosity materials was inspired by the chemical specificity inherent to biological systems. On the basis of the work of Pauling and Campbell[10] in which artificial antibodies were prepared using antigen molecules as templates, Dickey[11] prepared a selective adsorbent using a sol−gel process in which the silica network was formed in the presence of the target compound (in this case methyl orange) intended to be adsorbed. According to Dickey, during gelation, the silicate species were tightly organized around the methyl orange molecules due to noncovalent interactions such as van der Waals forces, hydrogen bonding, and interionic attractions. After washing the dried gels (*xerogels*) with MeOH to extract most of the methyl orange, adsorption studies showed preferential selectivity for methyl orange over its homologues—ethyl, *n*-propyl, and *n*-butyl orange.

Dickey's 1949 publication appears to be the first documented demonstration of molecular "imprinting" or "templating" to control pore size and shape. Since then molecular and supramolecular templating have been used to synthesize a broad range of organic and inorganic materials. In the broadest sense a template may be defined as a central structure about which a network forms in such a way that removal of the template creates a cavity with morphological and/or stereochemical features related to those of the template.[12] A general template approach is illustrated in Figure 1, where primary structural units are organized around a molecular template and solidified to form a matrix. The fidelity of the imprint created by template removal depends on several factors: (1) the nature of the interaction between the template and the embedding matrix; (2) the ability of the matrix to conform to the template; (3) the relative sizes of the template and the primary units used to construct the matrix.

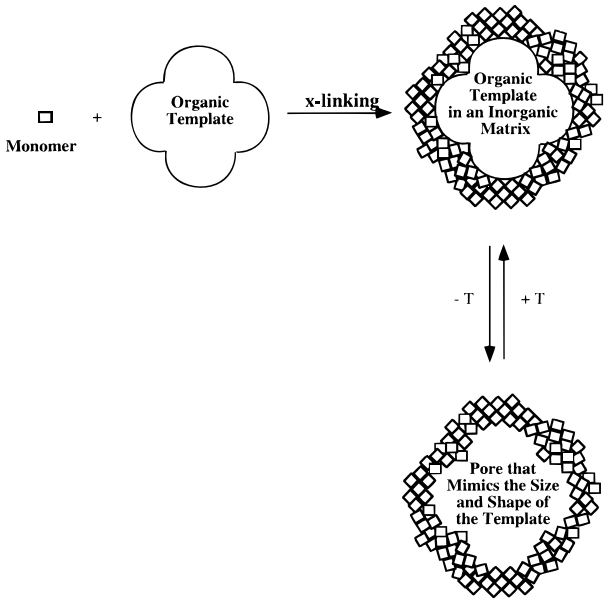

Figure 1. Schematic of the organic template approach to prepare nanoporous amorphous silica showing the incorporation and removal of the template.

To ensure intimate association of the template with the matrix, Wulff and co-workers[13] devised synthesis schemes in which functional groups were bound revers-

[†] University of New Mexico.
[‡] Sandia National Laboratories.
* Corresponding author. Tel: +1 505 272 7627, Fax: +1 505 272 7304.
[⊗] Abstract published in *Advance ACS Abstracts,* July 15, 1996.

S0897-4756(96)00138-X CCC: $12.00

ibly to a template as polymerizable vinyl derivatives. The derivatized template molecule was then co-polymerized with added monomer and cross-linking agents to form a highly cross-linked matrix. Template extraction created cavities possessing a shape and stereochemical arrangement of functional groups corresponding to that of the template. Sellergren and co-workers[14] developed a simplified procedure based on noncovalent interactions of the template and matrix. The template was assumed to interact by a combination of electrostatic interactions and hydrogen bonds with monomer (methacrylic acid) prior to polymerization and after polymerization with the carbonyl groups of the poly(methyl methacrylate) matrix. Enantiomer selective adsorbents for amino acid derivatives were produced by this method,[14] and it was observed that templates containing a higher number of interaction sites resulted in polymers of higher selectivity.[15]

Close association of template and inorganic precursors is vital for successful templating of inorganic materials as well. For example, in studies of tetraalkylammonium- and hexanediamine-mediated syntheses of pure silica zeolites, Burkett and Davis[16,17] have used $^{1}H-^{29}Si$ CP NMR to show that organic−silicate complex formation via favorable van der Waals interactions is influential in directing zeolite crystallization. When $^{1}H-^{29}Si$ CP NMR signatures were not observed, the occluded organic molecule served to create a cavity, but there was no unique relationship between the template molecule and the resulting crystal phase. In the formation of ordered mesoporous silicas using supramolecular surfactant templates,[18] Stucky et al.[19] identified multidentate binding of silicate oligomers to the cationic surfactant and charge density matching between the surfactant and silicate as key factors in the precise templating of the silica by the surfactant assembly.

The importance of the ability of the matrix to conform to the template is evident from comparisons of amorphous and crystalline templated media. Whereas there exist many examples of imprinted organic polymers exhibiting size and shape selectivity,[13−15,20] including the ability to resolve chiral racemates, only in rare instances has an organic molecule been used to produce a zeolite whose internal cavities conform rigorously to the molecule shape—the triquaternary amine-mediated synthesis of ZSM-18 being the best example.[21] In the case of zeolites, it is likely that the constrained geometries and rather poor packing efficiency of the various cyclic species (e.g., double four-, five-, or six-rings of alternating silicon and oxygen atoms) that serve as oligomeric building blocks inhibit precise molding of the framework by the template.[12] On the other hand the wide range of network conformations available to organic polymers and polysiloxanes facilitate conformation about the template and promote custom-tailoring of pore size and shape.

Finally, it is evident that as the size of the template diminishes with respect to that of the primary structural units, the imprinted cavity will contain less morphological and stereochemical information. Whereas it would be easy to distinguish between family members on the basis of their footprints molded into beach sand, it would be difficult to differentiate their busts molded in bowling balls. Thus as the size of the intended imprinted feature approaches atomic dimensions, the registration between the template and network is bound to become less precise.

This paper discusses molecular and supramolecular templating of amorphous silicas from a materials processing point of view. In contrast to prior work in organic polymers aimed at producing molecular imprints on the surfaces of macroporous polymers for chromatographic separations, our discussion focuses on systems in which porosity is created solely by template removal for such applications as membrane-based separations and chemical sensing. In addition to the issues discussed above relevant in general to template-mediated syntheses of porous materials, materials for use as membranes require both accessibility and connectivity of the porosity.

We consider two classes of materials prepared from soluble precursors distinguished by the nature of the template−matrix interactions and the extent to which drying and heating is influential in dictating the final pore morphology. First we discuss the formation of silicas templated by surfactant molecules and supramolecular surfactant assemblies where the nature of the template−matrix interaction is via noncovalent bonding mechanisms such as electrostatic attraction, van der Waals contact, and hydrogen bonding, and the pore structure is for the most part established prior to drying and template removal. We then discuss porous silicas templated by organic ligands and polymers covalently bonded to the siloxane framework. In this class of materials, we show that both drying and heating strongly influence the final pore structure.

1. Noncovalently Bonded Organic Templates

1.1. Introduction. Noncovalently bonded organic templates include molecules, polymers, and supramolecular arrays. When dissolved in solution these species can template small inorganic groups via electrostatic, van der Waals, and hydrogen-bonding interactions to form nanostructured materials with tailorable pore shapes and sizes. Two primary examples of silicates whose structures are directed by noncovalently bonded species are molecular sieves,[22] e.g., silicalite, and periodic mesoporous silica,[18,23−25] e.g., MCM-41. In the case of molecular sieves the relative importance of the different interactions in directing structure is still a matter of debate.[26,27] In periodic mesoporous silica synthesized from charged surfactants, electrostatic interactions are thought to have a decisive role in the initial organization of the inorganic−surfactant array.[28] For neutral surfactants, hydrogen-bonding interactions are likely decisive.[29]

In zeolites, the organic molecule rarely acts as a true template but typically directs structure or fills space in the porous product. The ability of the organic molecules to rapidly rotate in solution combined with the comparable atomic sizes of the organic molecule and the framework building units generally result in a rather indirect correlation of the shape and size of the organic molecule to the structure and volume of the cavity created in the inorganic framework.[26,27]

In contrast, in silica mesophases the organic group clearly acts as template. There is a direct correlation of the surfactant array size and shape to the final pore size and geometry in the mesophase. The intimate template−matrix association is facilitated by the flex-

ibility and compliance of an inorganic network built up of relatively small silicate oligomers and by the large radius of curvature of the organic template. For example, if the final pore diameter of the mesophase is 40 Å, then the circumference of a circular cross section is ~125 Å; a silicate chain that rings the circumference, contains ~31 monomeric silica species. The relative size difference of the building blocks and the wide variety of bond angles and conformations available to the amorphous (and initially poorly condensed) framework allows the matrix to tightly conform to the template.

A wide variety of uses for periodic mesophases have been demonstrated or contemplated, including use as acid catalysts[30−32] (although acidity is less than for zeolites),[33,34] oxidative catalysts for bulky organics,[35−37] alkylation catalysts for large molecules,[38] shape-selective polymerization of organic polymers,[39] supports for noble-metal oxidation and hydrogenation catalysts,[37] supports for NiMo in hydrocracking applications,[40] supports for heteropolyacid ion catalysts,[41,42] supports for catalytically active organometallics,[43] hosts for conducting polyaniline filaments[44] and carbon wires,[45] hosts for organometallic clusters that can be decomposed to metal clusters,[46] miniature reactors for electron-tranfer reactions,[47] coatings for sensors,[48,49] and high surface area adsorbents.[23]

Control of pore geometry and diameter are key to many of these applications, especially those that rely on size and/or shape selectivity and ready access to porosity. As discussed in detail below, pore geometry is controlled primarily by the concentration of surfactant in solution and by the processing conditions. Pore size is controlled by the length of the surfactant, addition of auxiliary organics, choice of solvent, template removal method, aging conditions, processing conditions, and postfunctionalization of the isolated porous material. The thickness of the inorganic walls, which can affect the stability of the materials, is controlled by the charge of the surfactant and the formation mechanism. Before we can understand how to engineer pore sizes and shapes, we must understand the components that make up the mesophase and how they are assembled.

1.2. Surfactant Templates. *Definition and Aggregation.* Surfactants are bifunctional molecules that contain a solvent-loving (lyophilic) head group and a solvent-hating (lyophobic) tail (i.e., they are amphiphiles).[50] As a result of their amphiphilic nature, surfactants can associate into supramolecular arrays. For example, cetyltrimethylammonium bromide ($CH_3(CH_2)_{15}N(CH_3)_3^+Br^-$ or C_{16}TMABr) in water will form spherical micelles that contain ~90 molecules. In the micelle, the hydrophilic head groups form the outer surface and the hydrophobic tails point toward the center. This arrangement minimizes the unfavorable interaction of the tails with water but introduces a competing unfavorable interaction, the repulsion of the charged head groups. The balance between these competing factors determines the relative stability of the micelles.

The extent of micellization, the shape of the micelles, and the aggregation of micelles into liquid crystals depends on the surfactant concentration. A schematic phase diagram for a cationic surfactant in water is shown in Figure 2. At very low concentration, *c*, the surfactant is present as free molecules dissolved in solution and adsorbed at interfaces. At slightly higher concentrations, called the critical micelle concentration (CMC1), the individual surfactant molecules form small, spherical aggregates (micelles). At higher concentrations (CMC2), where the amount of solvent available between the micelles decreases, spherical micelles can coalesce to form elongated cylindrical micelles.

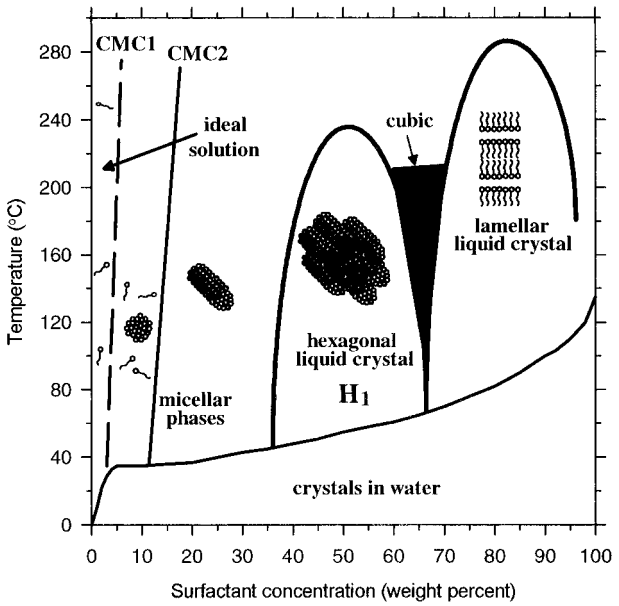

Figure 2. Schematic phase diagram for C_{16}TMABr in water. CMC1 is exaggerated to higher concentration.

Table 1. Expected Micelle Structure for Different Critical Packing Parameters

CPP	types of surfactants	expected aggregate structure
<0.33	single chain, relatively large heads	spherical or ellipsoidal micelles
0.33−0.5	simple surfactants with relatively small head groups; ionics with high electrolyte concentration	relatively large cylindrical or rod-shaped micelles
0.5−1.0	double chains with large heads	vesicles or bilayer structures

At slightly higher concentrations, liquid-crystalline (LC) phases form. Initially, rodlike micelles aggregate to form hexagonal close-packed LC arrays. As the concentration increases, cubic bicontinuous LC phases form followed by LC lamellar phases. At very high concentrations, in some systems, inverse phases can exist. Here water is solubilized at the interior of the micelle, and the headgroups point inward.

A simple theory of micellar structure has been developed based on the geometry of micellar shapes and the space occupied by the hydrophilic and hydrophobic groups of the surfactant molecule.[51] The critical packing parameter (CPP) is defined as $V_H/a_o l_c$ where V_H is the volume of the hydrophobic portion of the molecule, a_o is the optimum headgroup area, and l_c is the critical length of the hydrophobic tail, which is typically: $l_c \leq 1.5 + 1.265n$ Å, where n is the number of carbon atoms in the chain, or one less (see Table 1). The exact value of l_c depends on the extension of the chain. The aggregate structure depends on the value of the CPP. The value of the CPP dictates the behavior of the surfactant in the precursor solution: the larger the value, the less the curvature in the aggregate. In general, simple, single-chain surfactants that have low

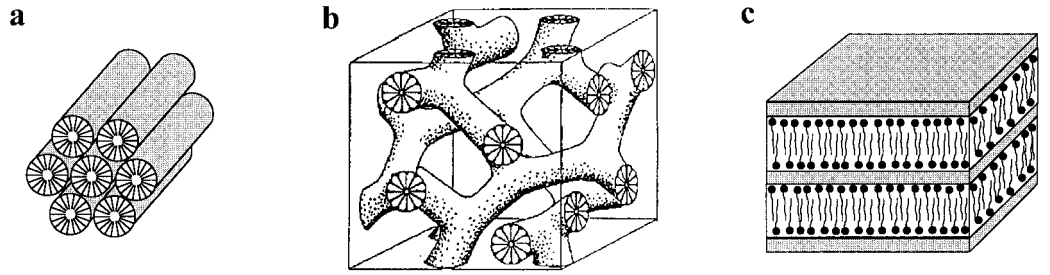

Figure 3. Three structure types observed for silica−surfactant mesophases: (a) hexagonal; (b) cubic bicontinuous, *Ia*3*d*; (c) lamellar.

values of CPP are employed in mesophase syntheses. Surfactants that have double alkyl chains are generally avoided as they have high values of CPP and tend to form lamellar mesophases.

Surfactant Types. Surfactants with a wide variety of sizes, shapes, functionalities, and charges have been used to form mesophases. The surfactants are classified based on their head group chemistry and charge: Anionic—the hydrophilic group carries a negative charge; examples include sulfates[52] ($C_nH_{2n+1}OSO_3$ (n = 12, 14, 16, 18), sulfonates[52] ($C_{16}H_{33}SO_3H$ and $C_{12}H_{25}C_6H_4SO_3$-Na), phosphates[52,53] ($C_{12}H_{25}OPO_3H_2$, $C_{14}H_{29}OPO_3K$), and carboxylic acids ($C_{17}H_{35}COOH$ and $C_{14}H_{29}COOH$). Cationic—the hydrophilic group carries a positive charge; examples include alkylammonium salts, such as ($C_nH_{2n+1}(CH_3)_3NX$, n = 6 (nonmesophase), 8, 9, 10, 12, 14, 16, 18, 20, 22; X = OH/Cl, OH, Cl, Br, HSO_4, and $C_nH_{2n+1}(C_2H_5)_3N$, n = 12, 14, 16, 18), gemini surfactants[52] [$C_mH_{2m+1}(CH_3)_2N-C_sH_{2s}-N(CH_3)_2C_mH_{2m+1}$]$Br_2$, m = 16, s = 2−12) cetylethylpiperidinium salts[52] ($C_{16}H_{33}N(C_2H_5)(C_5H_{10})^+$); and bichain salts[52] (dialkyldimethylammonium). Nonionic—the hydrophilic group is not charged; examples include primary amines ($C_nH_{2n+1}NH_2$)[29] and poly(oxyethylene oxides),[54] octaethylene glycol monodecyl ether ($C_{12}EO_8$), and octaethylene glycol monohexadecyl ether ($C_{16}EO_8$).[55] A fourth class, amphoteric (and zwitterionic), exists, but no reports of their use are known.

1.3. Synthesis of Surfactant/Inorganic Mesophases. To synthesize periodic mesoporous silica, four reagents are generally required: water, a surfactant, a silica source, and a catalyst. The silica source(s) dictates the reaction conditions. For nonmolecular silica sources, which include, fumed silicas, precipitated silicas, or water glass, a gel that contains all of the reagents is formed from a nonhomogeneous solution and is treated hydrothermally at ~75 to ~180 °C for several hours to several days.[23,34] Surfactant concentrations are typically ~15 to ~30 wt %.

When molecular silica sources,[52] which include alkoxysilanes, such as tetraethoxysilane (TEOS) or tetramethoxysilane (TMOS), are used, water, surfactant, and catalyst are first combined to form a homogeneous micellar solution. To this micellar solution the molecular alkoxide is added. The mesophase generally forms in seconds to minutes at temperatures as low as −14 °C. Surfactant concentrations as low as ~0.5 wt % can be used. A cosolvent such as methanol can be added to the precursor solution to ensure homogeneity and maximize product yield.[56]

As shown in Figure 3, pure silica mesophases, exhibit three structure types:[23] hexagonal (H; or MCM-41), a 1-d system of hexagonally arrayed cylindrical pores; cubic (C), a 3-d, bicontinuous system of pores (*Ia*3*d* and *Pm*3*n*); lamellar (L), a 2-d system of metal oxide sheets interleaved by surfactant bilayers (probably many closely related structures of this type). In the latter, the structure collapses when the template is removed, so it is of less interest. In each type there is a periodic arrangement of pores (or layers), but the inorganic walls (or sheets) are amorphous; see Figures 4 and 5. In addition a variety of less well ordered phases have been observed. These materials generally exhibit one low-angle diffraction peak and have narrow pore size distributions and high surface areas.[25]

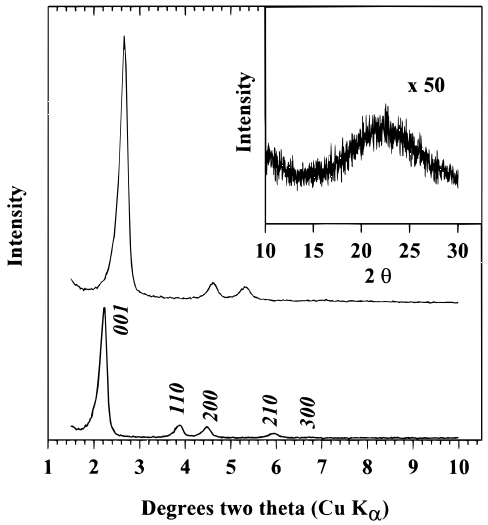

Figure 4. X-ray diffraction patterns of silicate mesophases showing the periodicity of the pore system: as-synthesized (bottom) from 1 TMOS:0.13 C_{16}TMACl:0.26 NaOH:96.8 H_2O:18.1 MeOH and after calcination at 550 °C for 2 h (top) in O_2 (4.4 °C/min heating rate). The cell constant shrinks 15.3% upon calcination and the long-range order decreases. Indexed Bragg reflections are shown. Inset shows the broad feature characteristic of the amorphous silica framework.

Although our focus is on silica frameworks, we point out that the surfactant-templated approach to periodic porous materials is quite general. A variety of inorganic oxide frameworks, some of which may have important technological applications, have been realized, including silica doped with Al,[18,23,33,34,57−59] Ti,[35,36] V,[60] B,[61] Fe,[62] Mn,[63] Ga[64] (all H and C for Al and Mn) and transition-metal and main-group materials based on tungsten oxide (H),[66] antimony oxide (H, C),[66] titanium oxide (H),[52] zirconium oxophosphate,[65] and zirconium oxide (H),[37] vanadium oxide (H),[66] vanadium phosphate (H),[67] and tantalum oxide (H).[68] In addition, a large number of lamellar mesophases have been synthesized including those based on Si, Zn, Pb, Fe, Mg, Mn, Co, Ni, Al, and Ga oxides[52] and Sn,[52,69] W,[70] and Mo[70] sulfides.[70]

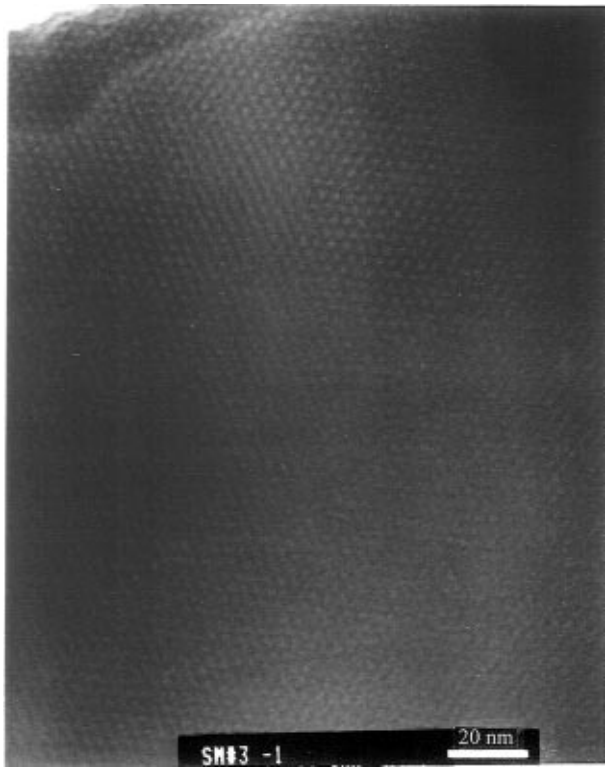

Figure 5. Transmission electron micrograph of a silica−surfactant mesophase showing the regular hexagonal arrangement of pores (light); the darker portion is the silica network.

In mesophase syntheses, the nature of the surfactant−matrix interaction is dictated by the reagents and the synthetic conditions and can affect the physical and chemical properties of the product. Six templating pathways[25,29,71] have been identified: S^+I^-, S^-I^+, $S^+X^-I^+$, $S^-X^+I^-$, S−I, and S°I°, where S is the surfactant, I is the inorganic phase, and X is the mediating ion. Silicates have been synthesized by S^+I^-, $S^+X^-I^+$, and S°I° pathways. As described above for an S^+I^- approach, a cationic surfactant is chosen and the pH is set such that the inorganic precursors will be negatively charged (pH of 9−14 for mesophases). For $S^+X^-I^+$ the synthesis is done well below the isoelectric point of silica (pH ∼ 2). For S°I° the reaction is done at near-neutral pH, which means the silicate ions are partially charged, but the amine is neutral.

The diverse reaction conditions that yield isostructural products, in addition to the existence of six synthetic routes, demonstrate that isostructural products can form from a broad spectrum of inorganic species, including fumed and precipitated solids, sols, salts, and alkoxides, and surfactant types, including single- and double-chain gemini, charged and neutral, and that the surfactant molecules can exhibit a wide degree of initial aggregation.

1.4. Formation Mechanism. There are two general methods used to synthesize silica/surfactant mesophases: (1) assembly of dissolved silica sources around surfactant arrays; (2) intercalation of surfactant ions into layered silicates. For the first general class, Mobil scientists[18,23] quickly observed that the resulting silica/surfactant mesophases strongly resemble mesophases seen in simple surfactant−water systems. This led them to postulate a liquid-crystal templating (LCT) mechanism[18,23] (Figure 6). They proposed two possible pathways. In the first, a surfactant liquid-crystal phase, H_1, exists in solution and serves as the template ($c = H_1$). Silicate species are deposited between surfactant tubules and then condense to form the inorganic network. In the second, the interaction of silicate species with the surfactants mediates the hexagonal ordering ($c < H_1$).

The LCT pathway by which a mesophase forms depends on the initial aggregation of surfactant and thus, according to the phase diagram (Figure 2) on the initial concentration of surfactant. Experimentally it is found that MCM-41-type phases form from micellar solutions in which the surfactant—before addition of the silica source—is initially all free ($c < CMC1$), in the form of spherical micelles ($CMC1 < c < CMC2$), in the form of cylindrical micelles ($CMC2 < c < LC$), or in the form of liquid-crystalline phase, such as H_1 ($c = LC$). The simple fact that MCM-41 can be formed by adding silica to the solutions implies that the silicate species can significantly or subtly change the system thermodynamics. The addition of silica effectively pushes the concentration axis in the phase diagram (Figure 2) to the right and dramatically expands the liquid-crystalline phase space in the solvent:surfactant:silica diagram (here MCM-41 is considered a silica/surfactant liquid-crystalline phase).

The case where $c = H_1$ corresponds to using a preformed liquid-crystalline array as the template for the inorganic phase, as described in pathway 1 (Figure 6). It is now clear that this is not the formation pathway in the initial Mobil work ([c] = 30 wt %).[18,23] Chen et al.[72] used in situ ^{14}N NMR to show that under the conditions used by Mobil scientists, preformed H_1 liquid-crystalline phases are not present in the synthesis medium and therefore are not the structure-directing agent. In later work,[73] Mobil scientists also concluded that for their synthesis temperatures and surfactant concentrations, preformed H_1 liquid crystals are not present.

An exciting recent discovery shows,[55] however, that this pathway may be operative when surfactant concentrations greater than 30 wt % are employed. With 50 wt % surfactant in water (i.e., octaethylene glycol monodecyl ether ($C_{12}EO_8$), octaethylene glycol monhexadecyl ether ($C_{16}EO_8$), or C_{16}TAB) liquid-crystalline phases form in solution. Adding TMOS ($TMOS:H_2O < 0.25$) to these phases and removing evolved methanol results in MCM-41-type hexagonal silica arrays. In this case the surfactant array appears to act as a cast or mold in which the inorganic network polymerizes through out the aqeous domains of the liquid-crystalline phase, and the formation of the ordered mesophase is effectively independent of surfactant:silicate interfacial interactions.[55]

In all other reports of MCM-41 synthesis the initial solution has $c < H_1$; this is the regime of pathway 2 (Figure 6). In these cases surfactant:silica interfacial interactions undoubtedly become increasingly important as we know that there are no liquid-crystalline phases in solution prior to addition of silica,[52,56,72,73] yet MCM-41 LC-type products form. This implies that silica and surfactant cooperatively organize into an organic−inorganic liquid-crystalline phase during the course of the reaction. However, the details of the mechanism are still controversial. Three models have been

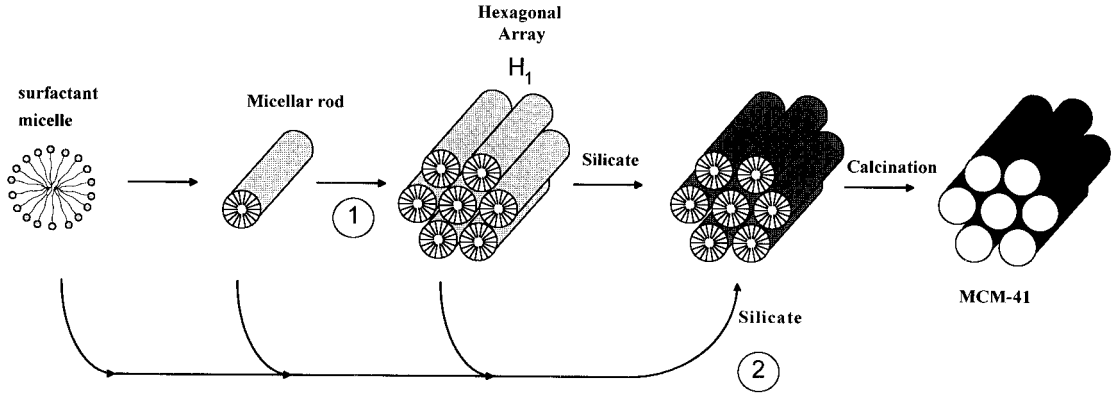

Figure 6. Schematic of the liquid-crystal templating (LCT) mechanism proposed in refs 18 and 23. Path 1 is liquid crystal initiated and 2 is silicate anion initiated.

postulated: puckering layered model (Steel et al.);[74] silicate rod assembly (Chen et al.);[72] cooperative charge density matching (Monnier et al.).[28]

The first model is based on ^{14}N NMR spectroscopy and X-ray powder diffraction data, and it assumes that the hexagonal surfactant mesophases are present and that silicate source dissolves into the aqueous regions around the surfactant arrays. These silicate sheets and hexagonal surfactant phases then give rise to hexagonal silica−surfactant mesophases via puckering of the silicate sheets.

The second model is based on X-ray powder diffraction, thermogravimetric analysis, ^{29}Si NMR, and in situ ^{14}N NMR spectroscopy of precursor solutions that have $c >$ CMC2. It proposes that randomly ordered, rodlike micelles form initailly and interact with silicate species to form surfactant rods encapsulated by 2−3 monolayers of silica; these species then spontaneously assemble into a hexagonal structure that has long-range order. The silicate species continue to condense with time and heating.

The third model was arrived at by studying synthetic solutions that have $c >$ CMC1 and has been clarified several times.[28,52,75] The model directly addresses syntheses from solutions that have surfactant concentrations < CMC2, and preparations where shorter chain surfactants (e.g., $n = 12$; X = OH or Cl)[18,23] that do not form rods are used. The mechanism involves[52] (1) cooperative nucleation of inorganic and organic species, (2) liquid-crystal formation with molecular inorganics, and (3) inorganic polymerization and condensation.

It assumes that when charged surfactants are used, the initial step is preferential ion exchange of the surfactant counterions with polycharged oligomeric silicate species. These silicate species serve as multidentate moieties and can bind several surfactant molecules and screen the repulsive forces between the headgroups within an aggregate. This can reduce the local curvature and allow the aggregate to grow in size. This type of effect is well documented in simple surfactant−water systems. For example, when electrolytes are added to C_nTMABr solutions, a spherical-to-cylindrical micellar transition is observed.[76−81] These types of interactions could certainly produce the silicate-encapsulated micellar rods described in the second mechanism.

The charge screening afforded by the silicate ions can reduce the thickness of the double layer that keeps the micelles separated. At the appropriate concentration, this can allow attractive interfacial forces to dominate the interaggregate repulsive forces and can induce self-assembly into a new ordered morphology. The ultimate structure and symmetry are determined by dynamic and often subtle interactions among the organic and inorganic species according to equilibrium thermodynamics.[75]

Regardless of the specifics of cooperative assembly, it appears clear that extensive condensation of silicate monomers and oligomers prior to MCM-41 formation is not necessary. In fact, when noncondensable inorganic species are used, organic−inorganic salt-like mesophases are formed. This led Firouzi et al.[75] to term MCM-41 type phases silicatropic liquid crystals (SLC). The SLC concept has been reinforced by experiments[75,82] that employ $Si_8O_{20}^{8-}$ cubic octamers. Firouzi et al. showed unambiguously with ^{29}Si NMR that the as-synthesized structures contain uncondensed cubic octamers (pure Q^3), which shows that condensation of the silicate framework is not essential to the formation of MCM-41.

In situ ^{2}H NMR data confirm that the resulting SLC is quite similar to a lyotropic liquid crystal (LLC) formed in the surfactant−water system except that the order parameter is increased in the SLC and the mobility of silicate polyanions is reduced compared to the Br^- ion in the LLC. The SLC nature is further illustrated by a reversible lamellar to hexagonal transformation in a purely Q^3 material. The hexagonal structure can be irreversibly achieved by heating for 24 h at 70 °C to condense some of the silica ($Q^3/Q^4 \sim 1$).

Fyfe et al.[82] showed that the octamer could be used to directly synthesize lamellar and hexagonal phases. Reducing the framework charge by titrating the oxoanions with acidic vapor, leads to step-by-step structural transformations: layered precipitate (L_o) → cubic (V_1, $Ia3d$) → lamellar (L_1) → hexagonal (H). The facile transformation from one structure to another again demonstrates the liquid-crystalline nature of the phases. The transformations are performed at 105−130 °C and generally lead to the condensation of silicate species and thus are not reversible.

Mobil scientists have studied the role of surfactant chemistry in the formation of microporous and mesoporous molecular sieves to validate their LCT mechanism.[73] Products prepared under identical conditions from a series of alkylammonium surfactants C_nTMABr, $n = 6, 8, 10, 12, 14, 16$, showed that (1) at temperatures from 100 to 200 °C, amorphous or microporous (zeolitic)

materials form when $n = 6$ (2) at 100 °C MCM-41 type materials form when $n = 8-16$, (3) at 150 °C MCM-41 forms when $n = 10-16$, zeolitic phases were produced when $n = 8$, and (4) at 200 °C amorphous and zeolitic phases form when $n = 8-16$.

The results show that there is a correlation of CMC with the ability to form MCM-41 and with product periodicity.[83] Surfactants with $n \leq 6$ do not form micelles in aqueous systems and do not form MCM-41 in the presence of silica. Surfactants with $n = 8-16$ form MCM-41, but the product periodicity, as judged by the number of peaks and their widths in the XRD pattern, increases significantly as n increases. Micellization is favored at lower and lower concentrations as n increases (CMC1 drops by over 2 orders of magnitude ($n = 8$ (0.14 M)[84] versus $n = 16$ (0.00092 M)[85]). Thus as the favorability of micellization and the size of hydrophobic portion of the molecules increase, product periodicity increases.[86] The change in product type from MCM-41 at 100 °C to zeolitic phases at 150 °C for $n = 8$ again reflects the decreasing favorability of micellization (increase in CMC) as temperature increases and likely leads to the inability to form MCM-41.

Cheng et al.[87] examined whether it is necessary to have any preorganization (micellization) of the surfactant in solution to form ordered mesophases. They claim that MCM-41 can be synthesized with surfactant concentrations as low as, but not below, CMC1. Anderson et al.[56] used static light scattering, X-ray diffraction, and TEM to show that mesophases which are stable to calcination can be made with C_{16}TMABr below CMC1 in water−methanol systems but that their long-range order is not as great as for materials made above CMC1. This implies that as long as the surfactant acts as a chemical dipole when the silica source is added, preorganization of the surfactant (micellization) is not necessary; however, preorganization is beneficial to long-range order.

To conclude the discussion of LCT pathways, it is important to point out that none of the models explicitly address the case where strong electrostatic interactions are absent, as is the case for neutral surfactants. Neutral surfactants have a much greater tendency to form aggregates in water than charged surfactants as evidenced by their ~2 orders of magnitude smaller CMC1s for the same number of carbons in the alkyl chain.[50a] Apparently the strong tendency of the surfactants to aggregate in combination with hydrogen-bonding interactions is sufficient to allow the formation of mesophases. In parallel with electrostatically templated materials, neutrally templated silicates with high concentrations of surfactant show better long-range order than low concentrations.

The second general formation mechanism assumes the intercalation of surfactants into the layers of the kanemite structure[88] followed by conversion into an MCM-41 type structure.[89−91] A "folded sheets" mechanism has been implicated here.[92] Similar conversions may take place in lamellar structures synthesized from solution that are converted to hexagonal structures.[28]

1.5. Controlling, Creating, and Accessing Porosity. The pores in mesophases are about an order of magnitude larger than for zeolites and can be tailored within the ~1.5 to ~10 nm range. Mesophases exhibit specific surface areas greater than 1000 m^2/g, pore volumes greater than 0.5 cm^3/g, benzene sorption capacities up to 67% by weight at 50 Torr and 25 °C, and, owing to the regularity of the templates, a unimodal, narrow distribution of pore sizes (see Figure 7). Sorption isotherms on a wide variety of gases, including N_2,[18,23,93,94] O_2,[93,94] Ar,[95] H_2O,[96] SO_2,[96] CO_2,[96] cyclopentane,[97] and benzene[23] have been measured for this model absorbant. After the template is removed, pure silica MCM-41 adsorbs a much greater amount of organic species than water[34] (>0.4 g/g for cyclohexane and <0.05 g/g for water at $P/P_0 = 0.4$), which reveals that the internal surfaces are quite hydrophobic even though there are silanol groups present ($Q^3/Q^4 \sim 0.25$).[23] Trimethylsilylation renders the materials repellent even to liquid water.[98] The long-range 2-d order of the pores as calculated from X-ray diffraction data can vary widely depending upon surfactant concentration, silicate source, and preparation conditions.[25]

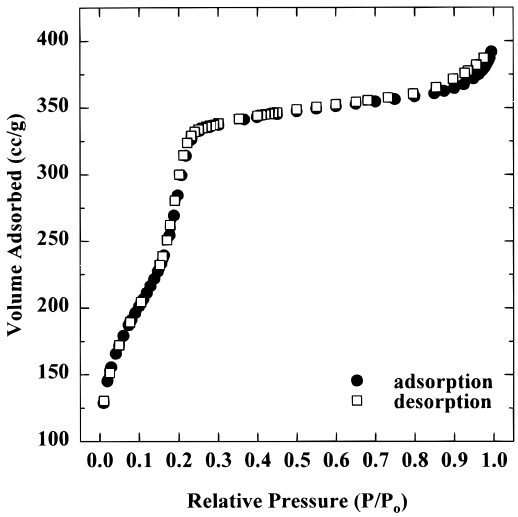

Figure 7. N_2 sorption isotherm collected at 77 K on the calcined sample shown in Figure 4. The steep uptake at low P/P_0 is characteristic of the narrow pore size distribution found in calcined periodic mesophases. The surface area of the sample is 902 m^2/g, the pore volume is 0.61 g/cm^3, the pore diameter is ~27 Å, and the wall thickness is ~11.5 Å. The fwhm of the pore size distribution is ~4 Å.

Three general steps are involved in forming porous amorphous silica: synthesis, drying, and template removal. A fine degree of control over the pore diameter in MCM-41 is afforded in the synthesis by the type of reagents used, the synthetic conditions employed, and the aging conditions. Once the materials are isolated, however, their structure and pore connectivity are essentially fixed. Drying MCM-41 results in little shrinkage of the network and thus has little affect on porosity. This stands in sharp contrast to amorphous microporous materials, where drying largely controls the ultimate pore diameter and connectivity as described in subsection 2. The method and conditions used to remove the template affect the final volume fraction porosity and the pore size of the materials, but (except under extreme conditions) not the connectivity or arrangement of the pores. A coherent picture of how to control the porosity from step to step (synthesis to drying to template removal) has not yet emerged; however, aspects that affect porosity have been studied individually; see Figure 8.

A. Surfactant Chain Length. Crude control of pore size in the metal oxide−surfactant composite is afforded

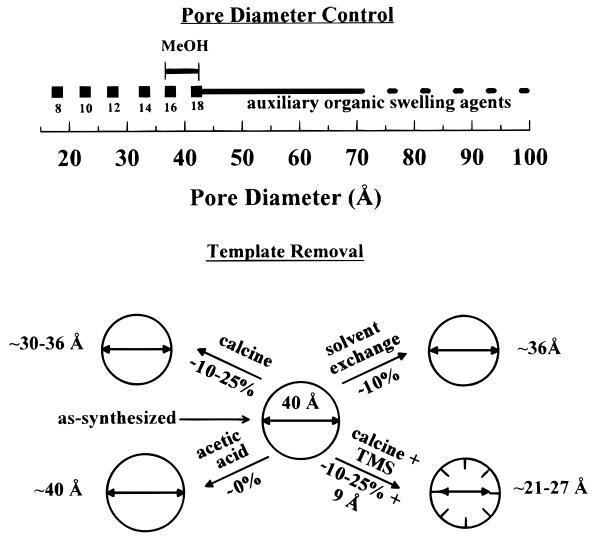

Figure 8. Top shows a schematic of synthetic approaches to control pore diameter. For pores between ~15 and ~45 Å, the number indicates *n* in C_nTMABr for as-synthesized samples (from ref 48 and extrapolation). MeOH shows the continuous control of pore diameter achievable by adding a cosolvent to the precursor solution. For pores greater than 45 Å, auxiliary organics are added to achieve regular pores up to ~70 Å and irregular pores up to 120 Å. Pore diameter was calculated by subtracting 10 Å (wall thickness) from the measured cell parameter. Bottom shows a schematic of the effect of template removal method and conditions on a sample with an initial nominal 40 Å pore diameter. Percentages indicate shrinkage.

simply by changing the length of the surfactant tail. For example, in the series C_nTMABr, $n = 8$, 10, 12, 14, 16, 18, the pore size of the as-synthesized material increases about 2.25 Å for each increase of one carbon in the surfactant.[23,66] Even-numbered carbon-chain-length surfactants are readily available, so the pore size can be conveniently stepped in ~4.5 Å increments. The shortest chain surfactant from which mesophases can be made is $n = 8$. The lower limit of pore size is thus ~15 Å. Owing to the limited solubility and high melting point of surfactants with $n >$ ~18 carbons, the practical upper limit of pore diameter that can be achieved by changing *n* is ~45 Å.

B. Adding Auxiliary Organics. Hexagonal mesophases can be made with regular pore diameters up to ~80 Å by dissolving hydrophobic molecules into the interior of the surfactant tubules that exist within a freshly made MCM-41 product prior to extensive condensation of the silicate framework.[99] The effects of a wide variety of such auxiliary organics have been investigated, including paraffins, aromatics, and alcohols.[99] The alkylated benzene 1,3,5-trimethylbenzene (TMB) provides a nearly linear increase in pore size with increasing concentration up to a TMB:Si ratio of 2.5. The maximum unit cell is ~65 Å by XRD; however, irregular pores up to ~120 Å have been imaged by TEM.[99]

C. Restructuring at Elevated Temperatures. Khushalani et al.[100] showed that siliceous mesophases could be restructured at elevated temperatures in alkaline solutions resulting in expansion in pore size from ~30 to ~70 Å. The pore wall thickness remains approximately constant at 6 Å over the 10 day anneal. The materials retain structural integrity when calcined at 540 °C.

D. Surfactant Type. The formation mechanism influences the long-range order and wall thickness of a mesophase. For example, silicate mesophases made from neutral amines ($c <$ LC) exhibit smaller coherent scattering domain (CSD) sizes (≤170 Å) and thicker framework walls (≥17 Å) compared to those made from charged surfactants (CSD commonly >900 Å; (walls ~8−13 Å).[29] In the case of neutral surfactants, strong electrostatic interactions are absent. It appears that such interactions are beneficial to long-range order, and that hydrogen-bond-mediated synthesis gives rise to product with thicker walls.

E. Cosolvents. Anderson et al.[101] studied the effect of a variety of alcohols, ethers, carboxylic acids, glycols, ketones, and amides on the structure of siliceous mesoporous materials. The type and concentration of cosolvent affect the pore diameter. For example, in the water:methanol solvent system, pore diameters can be continuously decreased over a ~5 Å range by decreasing the water:methanol ratio.[56] The cosolvent changes the solution thermodynamics, which changes either the packing or the number of surfactant molecules in the micelle and causes the pore size to decrease.

F. Materials Processing. Few controlled studies of the effects of reaction time, degree of framework condensation, or template removal conditions on porosity and microstructure have been published. From what has been published, we find that there are four methods[37] to remove the template: (1) solvent extraction, (2) calcination, (3) oxygen plasma treatment, and (4) supercritical extraction. The first two have been studied in some detail.

Acidic ethanol has been used to extract the organic groups from electrostatically templated materials. Chen et al.[34] report that ~100% of the organic materials can be removed by contacting MCM-41 with a 1 M HCl solution (liquid-to-solid ratio is 300 mL/g) at 70 °C for about 30 h. The cell contraction in the case of acidic ethanol is ~11% compared to the as-synthesized materials. This is attributed to the further condensation of silanol groups.

Pure ethanol at room temperature has been used to extract greater than 85% of the organic components from acid-synthesized ion-mediated ($S^+X^-I^+$) MCM-41.[66] Lattice contractions were not reported for this sample. Hot ethanol has been used to extract ~100% of the organic groups from a neutrally templated silica sample.[29] It appears that the unit cell size does not shrink in this case, but there is only one broad peak in the XRD pattern so it is difficult to accurately access the cell size. The extraction procedure is not expected to affect the wall thickness, thus, as the unit-cell size does not appear to change, the pore diameter does not change (cell constant = pore diameter + wall thickness); however, the concentration of silanol groups in pore walls does change.

MCM-41 samples have been calcined in flowing N_2, O_2, or air. Mobil scientists typically calcine at 540 °C in N_2 for 1 h and then in O_2 for 6 h.[18,23] The framework condensation increases from $Q^3/Q^4 \approx 0.67$ in as synthesized MCM-41 to ≈0.25 in the calcined sample.

Chen et al.[34] calcined MCM-41 samples at 540 °C in air for 10 h (heating rate = 1 °C/min). They observed up to a 25% decrease of the cell constant depending on synthetic conditions. This is in sharp contrast to

crystalline silicates which change very little upon heating;[34] for example, cubic Faujasite heated in to 500 °C in air undergoes a 0.3% volume increase whereas hexagonal Faujasite undergoes a 1.3% volume decrease under the same conditions.

In controlled experiments Chen et al.[34] heated four samples until framework collapse was evident. They found that as-synthesized materials are stable to ∼900 °C in air and the cell constant decreases by ∼23% at this temperature. The same sample extracted with ethanol is stable to ∼800 °C and the unit-cell constant decreases ∼24% total (11% after extraction and 13% upon heating). Previously calcined samples are stable to ∼800 °C when heated in dry air and ∼700 °C when heated in air with 8 Torr of water; the unit-cell constants decrease ∼26% and 23%, respectively. From these and other reports[23,52,56] it is apparent that the maximum shrinkage achievable before structural collapse under a wide variety of processing conditions is ∼25%.

The framework collapse observed at lower temperature when heated in water indicates that thermal stability of MCM-41 exceeds hydrothermal stability. Kim et al.[102] showed that the hydrothermal stability of aluminum doped (Si/Al = 39) mesophases could be increased by ion exchange in the order Y^{3+} (∼900 °C) ≈ Ca^{2+} > Na^{+} (800 °C) ≈ Al:MCM-41 > SiO_2 MCM-41 (∼710 °C).

Ryoo and Kim[103] add acetic acid to MCM-41 after it has reacted at 100 °C for 24 h. They adjust pH to 11 and repeat the procedure three times. The as-made and treated samples are then calcined in air for 2 h at 500 °C. The treated sample shows essentially no contraction of the unit cell as compared to a ∼25% shrinkage for an untreated sample. The BET surface area of the treated sample is 927 m^2/g, which, along with XRD, indicates the framework is still intact. ^{29}Si MAS NMR indicate that each successive acetic acid addition decreases Q^3/Q^4. The degree of framework condensation for the thrice treated sample changes little after calcination. The materials are stable up to 700 °C in humid air with 20 Torr of water.

G. Functionalization. Beck et al.[23] showed that trimethylsilylation of MCM-41 leads to a pore radius reduction of ∼4.5 Å. A wide variety of functionalizing groups have been used[99] including silanes, aluminum alkoxides, and combined Si−Al compounds, such as dialkoxyaluminotrialkoxysilane, boron, and phosphorus containing compounds. Maschmeyer et al.[43] showed that titanocene dichloride could be directly grafted to the inner walls of MCM-41. Morey et al.[104] showed that V centers could be grafted onto the walls of MCM-48 via impregnation of the host with vanadium isopropoxide in hexane to create $O_{3/2}V{=}O$ centers.

H. Creating Interparticle Porosity. Silicates with bimodal pore size distributions were made by Lin et al.[105] by calcining a wet mesoporous silica sample. The material contains two broad distributions of pore sizes d_{ave} ≈ 30 Å (fwhm ∼ 15 Å) and d_{ave} ∼ 110 Å (spread from 80 to 200 Å). Anderson et al.[106] synthesized monolithic periodic mesoporous silica gels that have a hexagonal array of ∼25 Å pores (pore volume ∼0.3 to ∼0.6 cm^3/g) and interparticle pores on the order of the particle size (∼150−500 nm). The interparticle pore volume can be tuned from ∼1 to ∼2.3 cm^3/g by varying the initial silica concentration or the drying conditions.

I. Accessing Porosity. MCM-41-type materials have been made in three useful forms: bulk powders,[18,23] monolithic gels,[105] and thin films.[48,49,107−109] The microstructure of the materials varies widely depending on the preparation conditions. For example, bulk powders generally form agglomerated 1−10 μm colloidal precipitates but can form spherulites, or aggregated submicron spherical particles. Monolithic gels can be formed from TMOS:water systems, and dried gels have bulk densities as low as 0.3 cm^3/g (0.02 cm^3/g before drying) and pore volumes >3 cm^3/g. High surface area hexagonal thin films can be made by in situ solution growth,[106] dip-coating a solution of premade particles,[48] gas-catalyzed synthesis,[49] or liquid−liquid interfacial reactions.[108]

1.6. Conclusions. Surfactants can be used to direct the structure in amorphous silica systems. If the surfactants have sufficient hydrophobic character, they can organize into supramolecular arrays and template the formation of liquid-crystal-like silica−surfactant nanostructures; otherwise they remain as free molecules and can structure-direct the formation of zeolites or can be incorporated in amorphous materials. In periodic mesoporous oxides, even though the pores are arrayed in a periodic fashion, the two primary components, that is, the surfactants within an array and the inorganic framework walls are not crystalline. The surfactant assemblies are akin to those in liquid crystals, and the metal oxide frameworks are amorphous. The relaxed configurational constraints and the large-pore diameters result in an inorganic network that conforms very closely to the size and shape of the final organic assemblage.

2. Covalently Bonded Organic Templates

2.1. Introduction. This section discusses organic templating of amorphous *microporous*[110] silica systems in which the templates are introduced as ligands covalently bonded to silica precursors. Several features distinguish the synthesis and processing of this class of materials from the mesoporous silicas described above: (1) Covalent bonding of the organic ligand to the inorganic framework forces close association of template and framework, limits the independent organization of the organic and inorganic moieties, and imparts hydrophobicity to the siloxane polymers and gel. (2) The framework initially established at the gel point exhibits low overall extents of condensation (Q^3/Q^4 = 1.6).[111] (3) The composite morphology continues to evolve beyond the gel point by processes such as syneresis, capillary shrinkage, relaxation, and sintering, so the nature of porosity created at the moment the organic templates are removed depends in a complex way on the preceding processing history. (4) In comparison to mesoporous materials, the much smaller template sizes required for micro- and ultramicroporous (d < 10 Å) materials requires there to be less perfect molding of the framework by the template.

2.2. Sol−Gel Processing. Sol−gel processing[112] offers a potentially simple method for the formation of microporous silicas[113] from molecular or oligomeric precursors. By growing rather weakly branched polymers, characterized by mass fractal dimensions less

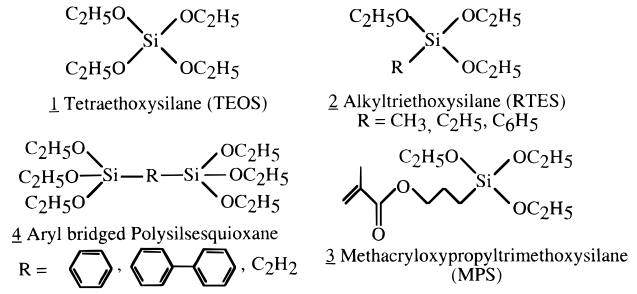

Figure 9. Examples of precursors used in the covalently bonded organic template approach showing matrix precursor (1), and pendant (2), polymerizable (3), and bridging templates (4).

than 2 and depositing films under conditions where the condensation rate is minimized and capillary stress is maximized, polymer interpenetration and collapse can be promoted to achieve pore sizes less than 1 nm in diameter.[114] Gels and thin films prepared with molecular sized pores have potential applications as catalyst supports,[115] adsorbents, sensors, and molecular sieving gas separation membranes.[116]

A potential disadvantage of this sol−gel approach, however, is that small pore sizes and narrow pore size distributions are achieved at the expense of pore volume.[84] Because aggregation and collapse of the polymeric species establishes the final pore size, the minimum achievable pore size is often determined by the competing effects of capillary stresses and increased network viscosity or modulus during drying.[82] The capillary stress causes the collapse of the network, while shrinkage and any accompanying condensation reactions stiffen the network resisting collapse. Under these conditions pore volume decreases as the pore size is reduced. The organic template approach in which molecules, ligands, or polymers are incorporated in a dense inorganic matrix and subsequently removed to create pores can overcome this limitation to pore volume.[87] The potential advantage of the organic template approach is that the organic ligand volume fraction may be used to control the volume fraction porosity of the network, independently of pore size, which depends on the template size and shape.

Organic templated microporous silicas are a subset of a larger class of hybrid organic−inorganic materials often formed by reacting mixtures of tetrafunctional alkoxides and organoalkoxysilanes under acidic or basic conditions.[117] The covalently bonded organic ligand is usually nonhydrolyzable and imparts partial organic character to an otherwise inorganic siloxane network. The organic ligands can be introduced as (1) pendant groups,[87,118−121] (2) bridging groups,[88,122−125] or (3) polymerizable groups[88,126] that can undergo organic polymerization either sequentially or simultaneously with the inorganic polymerization, forming mutually interpenetrating organic−inorganic networks (see Figure 9).

In addition to their ultimate role as pore size-directing templates, organic ligands introduced as pendant groups serve as network modifiers by reducing the functionality and therefore mechanical stiffness of the network and making the network more hydrophobic.[88] Organic ligands introduced as bridging groups may have the opposite effect on stiffness due to their higher functionality and possibly greater stiffness.[88,93,96] As we explain in the following sections, any reduction in mechanical stiffness of the network serves to promote the capillary stress-induced collapse of the gel network during drying, and to promote structural relaxation and densification during subsequent heat treatment. The hydrophobicity of the polymers and gel governs the interactions between the evolving condensed phase and the pore fluid during polymerization, aging, and drying and strongly influences both the tendency for phase separation and the magnitude of the drying stress.

To elucidate the role of covalently bonded template ligands in pore size direction, the following criteria must be satisfied:[87]

(1) The organic ligands must be uniformly incorporated in the inorganic matrix without aggregation or phase separation to avoid creation of pores larger than the size of the individual ligands.

(2) The synthesis and processing conditions should result in a dense embedding matrix (i.e., a network that wraps tightly around the template) so that the pores are created only by template removal.

(3) Template removal should be achieved without matrix collapse so that the pores created preserve the original size and shape of the template.[127]

(4) To ensure pore connectivity, it is necessary to exceed some percolation threshold of organic ligands.[87]

In the following sections we will discuss the criteria listed above in the context of the sequential stages of microstructural development of organic-templated amorphous silicas (Figure 10). Although the discussion is limited to amorphous silica, many of the issues addressed are common to hybrid organic−inorganic systems in general.

2.3. Uniform Incorporation of the Template Ligands. A necessary (but not sufficient criterion) for successful templating is to arrive at a uniform incorporation of the template in the silica matrix (stage c in Figure 10). A major challenge then is to avoid phase separation on all length scales. Phase separation in organic−inorganic systems shows striking similarities to phase separation in purely organic systems, i.e., it depends on the balance between unfavorable physical interactions such as hydrophobicity and favorable specific interactions such as covalent or H-bonding between the polymer and the solvent.[128−130] While it might be envisioned that gelation could be used to "freeze-in" a homogeneous state, phase separation can occur even after gelation on microscopic scales and diminish homogeneity.[131]

Several researchers have studied phase separation in organic−inorganic silica sols using ^{29}Si and ^{17}O NMR,[132] scanning electron microscopy[133] (SEM) and small-angle X-ray scattering (SAXS).[97,102] On the basis of ^{29}Si NMR, SAXS, and FTIR results, Coltrain et al.,[134] concluded that the tendency for phase separation in organic−inorganic silica sols could be reduced by the following approaches: (1) choice of the alkoxide ligands and reaction conditions to achieve comparable hydrolysis and condensation rates of the tetraalkoxysilane and organoalkoxysilane and therefore promote cross-condensation reactions, (2) development of strong interactions (e.g., via hydrogen bonding and van der Waals contacts) between the organic moieties in the silica network and the solvent and, (3) use of solvents that maintain favorable solvent−polymer interactions for the growing hybrid polymers.

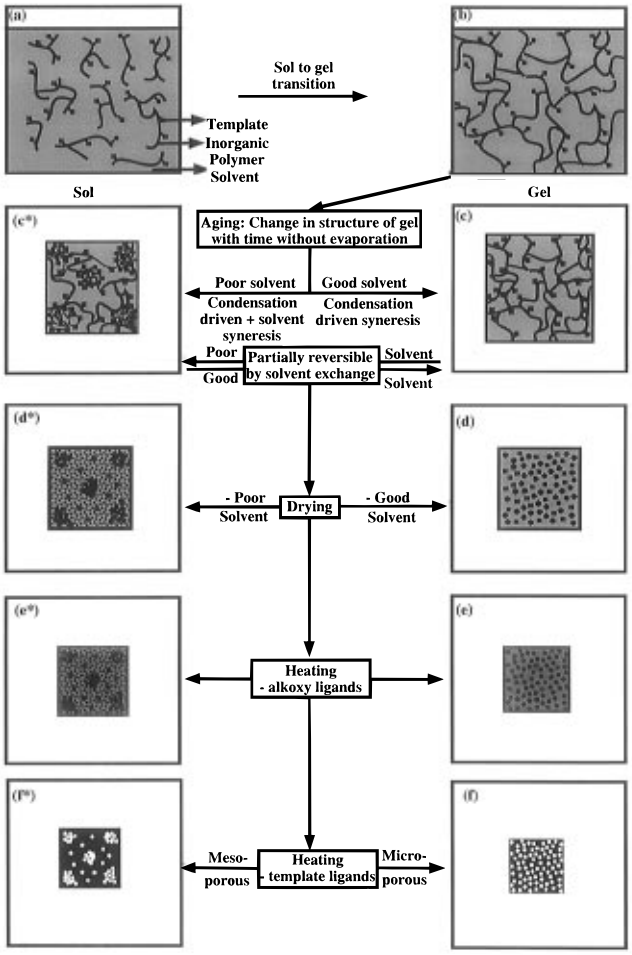

Figure 10. Schematic of the covalently bonded organic template approach to the formation of nanoporous amorphous silica, showing the effects of reaction, gelation, aging, drying, and template removal steps on the microstructure.

2.3.1. Reaction Rates. Similar reaction rates between the organoalkoxysilane and tetraalkoxysilane moieties, promote the formation of a network in which the templates are randomly distributed,[88] while preferred heterocondensation rates promote isolation of the organics within the inorganic network. Both inductive and steric factors are known to strongly influence the hydrolysis and condensation rates of organoalkoxysilanes.[83] Therefore to encourage heterocondensation,[83] the steric bulk of the alkoxide ligands introduced by the constituent alkoxides can be tailored to compensate for any accelerating or retarding inductive effects imparted by the template ligands, thereby promoting random or even preferential heterocondensation.[104] More effective condensation catalysts such as transition-metal alkoxides which increase condensation rates by several orders of magnitude can also be used to promote random heterocondensation—the idea being the "freezing-in" of a kinetically limited random configuration.[88]

Kinetics of hydrolysis and condensation (both self- and cross-) have been studied in MTES/TEOS,[102] ethyltrimethoxysilane/tetramethoxysilane (ETMS/TMOS),[135] MPS/TMOS,[97] and PTES/TEOS,[136] systems using ^{29}Si, ^{17}O, ^{1}H, and two-dimensional ^{1}H/^{29}Si NMR[137] and viscosity measurements[138] for a wide range of pH conditions and water/silicon (r) ratios. Spectroscopic techniques such as IR and Raman spectroscopies have also been used to evaluate the rate constants for hydrolysis and condensation in the MTMS/TMOS[139] and other alkyltrialkoxysilane[140] systems. Because the reactivity of alkyltrialkoxysilanes is very low in basic media, in contrast to pure silicon alkoxides, most studies of reaction kinetics have been performed in acidic conditions where the reactivity of all the precursors are better-matched.[88] Although ^{29}Si NMR peak assignments have been made for pure organoalkoxysilanes such as MTES,[141] reports on peak assignments of self- and cross-condensed products in mixed systems are relatively rare. Furthermore, the high r ratios used in typical sol−gel synthesis result in large extents of reaction, that broaden the ^{29}Si NMR resonances.[83]

Self- and cross-condensation reactions have been studied in acid-catalyzed 50 mol % RTES/TEOS (R = methyl, ethyl, phenyl) systems at low r ratios (0.5), using ^{29}Si NMR.[102,142] Because of the low r ratio, the main condensation products expected in these systems are the first condensation products, Q^1 and T^1, where Q and T represent silicon introduced as TEOS and RTES, respectively, and the superscript corresponds to the number of bridging oxygens attached to silicon. Peak assignments were made by comparing the resonances in the mixed system with those present in the pure TEOS and RTES spectra. On the basis of ^{29}Si NMR and ^{17}O NMR results, Prabakar et al.[102] concluded that (1) the cross-condensation products are formed in the early stages of the reaction in all the RTES/TEOS systems, (2) the relative rates of hydrolysis of the RTES silicon compared to the TEOS silicon determined the concentration of self- and cross-condensation products (i.e., the concentration of TQ was greater than TT or QQ in ETES and PTES systems, whereas it was identical in the MTES system which hydrolyzes much faster than TEOS), and (3) assuming condensation to occur only between dimeric species, the rate constant for cross-condensation was found to lie between the rate constants for self-condensation of the two monomers.

2.3.2. Polymer/Solvent Interactions. At higher r ratios and large extents of reaction, all the RTES/TEOS systems exhibit a marked tendency toward phase separation.[88,112] The influence of polymer solvent interactions on the tendency for phase separation is evident from studies of organotrialkoxysilane (RTES)/TEOS systems prepared with differing organic ligands and differing RTES/TEOS ratios.[143] For two-step acid-catalyzed syntheses employing H_2O/Si ratios, $r = 5$, the tendency for phase separation increased with increasing RTES/TEOS ratios and extent of condensation and with decreasing temperature (see Figure 11). With the choice of R, the tendency for phase separation increased with increasing hydrophobicity of the organic ligand, Me < Et < Ph. Because of the broad signals due to the varied environments of silicon, it has been impossible to date to identify precisely the nature of the species in phase-separated sols using ^{29}Si NMR. However, the denser phase is usually soluble in nonpolar solvents and volatilizes on heating to 150−200 °C, implying that it consists mainly of low molecular weight cyclic species,[112] whereas the less dense phase is usually less condensed and exhibits a poor signal-to-noise ratio (implying a lower concentration of silicon).[144]

In general, lower reaction rates and thermodynamically controlled processing regimes promote phase separation, whereas faster reaction rates and kinetically

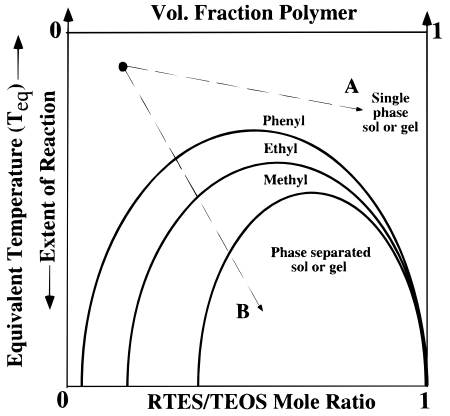

Figure 11. Schematic of the organic ligand type and concentration, and extent of reaction on macrophase stability in RTES/TEOS sols.

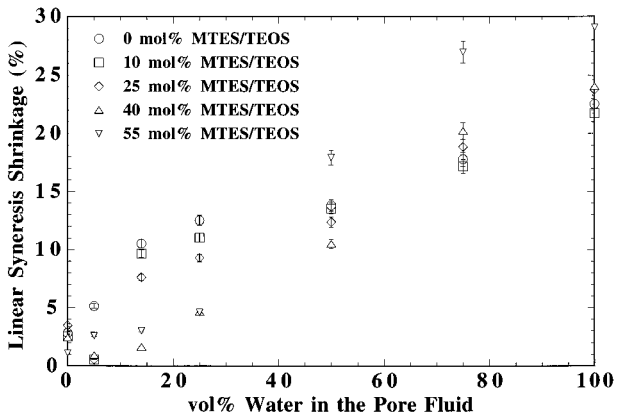

Figure 12. Syneresis shrinkage of MTES/TEOS gels as a function of MTES/TEOS ratio and pore fluid composition.

controlled processing regimes inhibit phase separation.[145]

2.4. Gelation and Aging. Gelation serves to freeze in a particular sol configuration. However, the structure continues to evolve, albeit on smaller length scales, after gelation—during aging.[83] The evolving microstructure reflects the complex interplay of the polymer and solvent as condensation proceeds.

Syneresis is defined as the spontaneous shrinkage of the gel due to the expulsion of solvent from its pores.[83,146] Syneresis in inorganic gels is attributed to continuing condensation reactions, and the syneresis rate is minimized at the isoelectric point of silica where the condensation rate is minimized. Syneresis occurs in organic—inorganic gels due to both continued condensation reactions and solid/liquid interfacial free energies which become more unfavorable as the extent of condensation increases. Syneresis driven by condensation reactions is generally observed to be irreversible.[83,116] For example, irreversible syneresis[116] was observed in pure TEOS gels to increase from about 1% in pure ethanol to 16% in pure water. In contrast syneresis driven by gel/solvent interactions is known to be at least partially reversible.[88] For example, organic gels are known to undergo reversible syneresis[147] with changing temperature, ionic strength, etc. Quinson et al.[148] observed that the pore size of titania gels shrunk from 7.5 to 3 nm when the solvent was changed from decane to water and reexpanded to its original pore size when reimmersed in decane. Syneresis in organic—inorganic gels can lead to vastly different shrinkage and microstructure, as depicted in Figure 10c and c*.

For hybrid systems in general, the RTES/TEOS ratio has several effects on syneresis:[149] (1) organic ligands reduce the connectivity of the network and thus its initial modulus K_0, (2) introduction of organic ligands causes the gel network to become progressively hydrophobic, and (3) organic ligands inhibit condensation reactions due to steric and solvation effects. The pore fluid water concentration has two related effects:[83,88] (1) water is generally observed to promote condensation reactions and (2) increased water concentration causes the solvent to become more polar reducing the solvent quality for hydrophobic polymers. Shrinkage results[119] presented in Figure 12 for MTES/TEOS gels as a function of increasing MTES and water concentration demonstrate the interplay of the polymer composition and pore fluid composition on syneresis. At constant MTES/TEOS ratios, all the gels exhibited progressively higher syneresis with increasing pore fluid water concentration. For example, syneresis of the 55 mol % MTES/TEOS gels increased from about −1.5% in pure ethanol to about 25% in pure water. Increasing the MTES/TEOS ratio from 0 to 55 mol % caused the shrinkage to increase in pure water from 22% to 29%, while in pure ethanol it caused ~1.5% expansion. About 14% of the shrinkage was reversible for the 55 mol % MTES/TEOS gels aged in water. Furthermore, skeletal density[119] of the 0 mol % MTES gels was found to increase with increasing water concentration consistent with condensation driven syneresis, while the skeletal density of the 55 mol % MTES/TEOS remained unchanged, implying that MTES inhibits condensation.

In summary, syneresis in organic—inorganic gels results from both condensation and gel/solvent interactions and is sensitive to the organic—inorganic ratio and the pore fluid composition. In general to promote homogeneity, it is necessary to age gels in solvents that promote favorable polymer—solvent interactions and inhibit condensation, so that the gel matrix shrinks and densifies during subsequent processing (see pathways c—f in Figure 10).

2.5. Drying. Syneresis is a self-limiting process. It slows down due to the decreasing network permeability and the stiffness of the gel which increases with shrinkage as a power law:[83,116]

$$K_p = K_0(V_0/V)^m \quad (1)$$

where K_0 and K_p are the initial and instantaneous bulk modulus of the gel, V_0 is the volume of the gel at gelation, V is the shrunken volume, and $m = 3.0-3.8$. To further densify the siloxane matrix it is necessary to remove the pore fluid by drying. There are several excellent reviews on the different stages of drying[150] and on application of drying theory to silica gels.[83] During the initial stages of drying, capillary tension develops in the pore liquid. The gel network, in response, shrinks to support this tension. Drying shrinkage stops when the increasing gel stiffness balances the capillary stress.[83] This balancing point is referred to as the critical point, because it establishes the final (dried) pore volume and pore size. The strain at the critical point,[83] ϵ, is given by

$$\epsilon = \{(1 - \phi_s)/K_p\}P_c \quad (2)$$

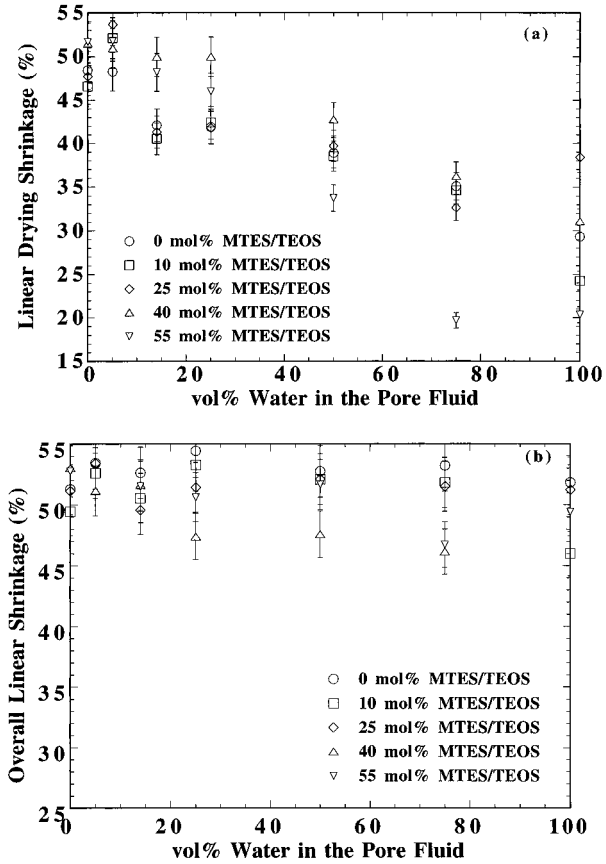

Figure 13. Drying shrinkage (a) and overall shrinkage (b) of MTES/TEOS gels as a function of MTES/TEOS ratio and pore fluid composition.

where ϕ_s is the volume fraction of solids and P_c is the maximum capillary stress at the critical point. During drying three situations exist: (1) if gelation precedes drying and K_0 is high, pores will probably empty and strain is described by eq 2, where P_c is given by the Laplace equation

$$P_c = -2\gamma \cos(\theta)/r_p \quad (3)$$

where γ is the vapor/liquid surface tension of the pore fluid, θ is the wetting angle, and r_p is the pore radius, (2) if gelation precedes drying and K_0 is low[151] (due to organic modification), the network may collapse sufficiently creating pores that are too small to empty at the relevant P/P_0, so P_c is given by the Kelvin equation

$$P_c = (RT/V_m)\ln(P/P_0) \quad (4)$$

where R is the ideal gas constant, T is the temperature, V_m is the molar volume of the pore fluid, and P_0 is the saturation pressure of the pore fluid, (3) if drying precedes gelation, e.g., during film formation, it is likely that situation 2 will prevail.[83] In addition, due to the hydrophobic nature of the gel and often the progressive enrichment of the pore fluid in water during drying, the contact angle will increase limiting the maximum capillary stress (eq 3) and therefore the drying strain (eq 2).

Because K_p increases due to both syneresis and drying shrinkage, the extent of drying strain (eq 2) will vary approximately inversely with the extent of syneresis shrinkage.[119] This is demonstrated in the comparison of Figures 12 and 13 which plot the syneresis shrinkage,

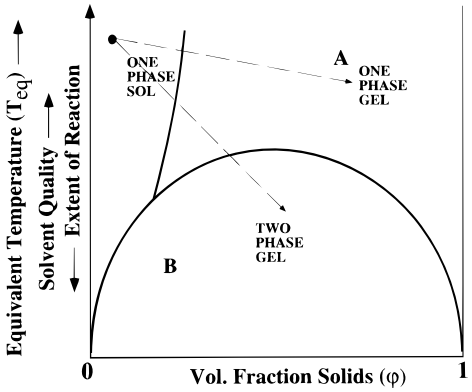

Figure 14. Equivalent phase diagram of a polymer gel in semidilute solution with a good solvent. From ref 123.

drying shrinkage, and total shrinkge for the same series of MTES/TEOS gels as a function of MTES/TEOS ratio and pore fluid water concentration. As drying proceeds, the volume fraction solids[83,101] and extent of condensation of the sol increase and, in mixed alcohol/water pore fluids, the pore fluid composition becomes enriched in water due to preferential evaporation of alcohol.[84,117,152] These combined factors are expected to promote phase separation of the gel as illustrated in Figure 14.[153] Continuing condensation reactions or diminishing solvent quality during drying cause the trajectory of the reaction path to cross the coexistence line (path B in Figure 14) rather than traverse the single-phase sol-to-gel phase boundary (path A). Although the cross-linking of the gel prevents macroscopic phase separation, the gel probably experiences at this point a "microphase separation" that increases the pore size and broadens the pore size distribution for equivalent extents of shrinkage.[101]

The linear shrinkage[119] of MTES/TEOS gels during drying is shown in Figure 13a as a function of MTES/TEOS ratio and pore fluid water concentration. The linear shrinkage of the gels during drying exhibited an opposite trend compared to syneresis, consistent with the physical and chemical changes that occurred during syneresis. For example, shrinkage of the 55 mol % MTES/TEOS gels decreased from ~50% when dried from pure ethanol to ~20% when dried from pure water. However, the overall shrinkage of the gels (including syneresis and drying) remained constant at ~50% (Figure 13b).

2.6. Microstructures of Dried Gels (Xerogels). The structure of the dried gels or *xerogels*, e.g., percent porosity and pore size, reflects the overall extent of shrinkage (eq 2) plus the extent of any microphase separation (stage c* in Figure 10) resulting from increased polymer concentration, extent of reaction, or preferential solvent evaporation (enrichment in nonsolvent). This section summarizes the general features of the microstructures of hybrid xerogels with respect to polymer/solvent interactions, drying rates (including thin film versus bulk), and the nature of the template ligand, e.g., bridging or pendant.

2.6.1. Effect of Polymer/Solvent Interaction. The effect of polymer/solvent interactions on xerogel microstructures is dramatically illustrated by the N_2 sorption isotherms shown in Figure 15 for 55 mol % MTES/TEOS gels dried from ethanol, 50 vol % H_2O/ethanol and water. Despite the fact that these gels exhibited about

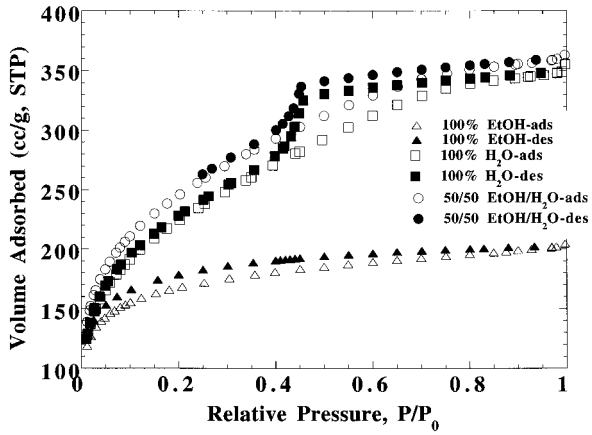

Figure 15. N_2 sorption isotherms of 55 mol % MTES/TEOS xerogels as a function of pore fluid composition.

the same overall extent of drying shrinkage (Figure 13b) they have considerably different microstructures.[119] The isotherm of the gel dried from pure ethanol is of Type I, characteristic of microporous materials. In addition, for a 5 s equilibration interval, the adsorption and desorption branch of the isotherm did not converge due to the slow kinetics of adsorption and desorption in the very small pores.[154] On increasing the pore fluid water concentration from 0 to 50 to 100 vol %, the isotherms change from Type I to Type IV that is characteristic of mesoporous materials, showing a net increase in the average pore size of the gels. The increase in average pore size is consistent with microphase separation similar to that illustrated in Figure 10 (stage c*).

2.6.2. Effect of Drying Rate. Faster drying rates, such as those that accompany film deposition, reduce the time scale for the competing interactions discussed earlier in the context of drying gels. Faster drying rates influence the final pore size in several ways:[83,122] (1) the short time scales significantly reduce the time available for condensation and phase separation and (2) the weakly condensed gels are more compliant and are more easily compacted, first by evaporation and then by the capillary pressure exerted at the final stage of the deposition process. Consequently, the pore sizes of films tend to be smaller than those of bulk gels. The effect of the drying rate on the microstructure of xerogels[87] is illustrated in Figure 16a. The 10 mol % MTES/TEOS xerogels that were dried slowly are microporous, characterized by a Type I isotherm for N_2. In contrast, the same sol prepared as a thin film on a surface acoustic wave substrate[114] exhibits a Type II isotherm consistent with a dense matrix or sufficiently small pores that measurable sorption does not occur at −196 °C.

2.6.3. Bridging versus Pendant Ligands. A major distinction between bridging and pendant organic ligands is that bridging templates serve to increase the connectivity of the network[93,96] and pendant ligands reduce the connectivity of the network. From the standpoint of drying, it is expected that bridging ligands will increase K_p and reduce ϵ (eq 2), resulting in more porous xerogels for equivalent organic loadings. This behavior is generally observed unless the bridging ligand is long and flexible, e.g., alkylene spacers with carbons >6 in which case the resulting xerogels have been reported to exhibit Type II N_2 isotherms and Type I CO_2 isotherms.[94,96,93]

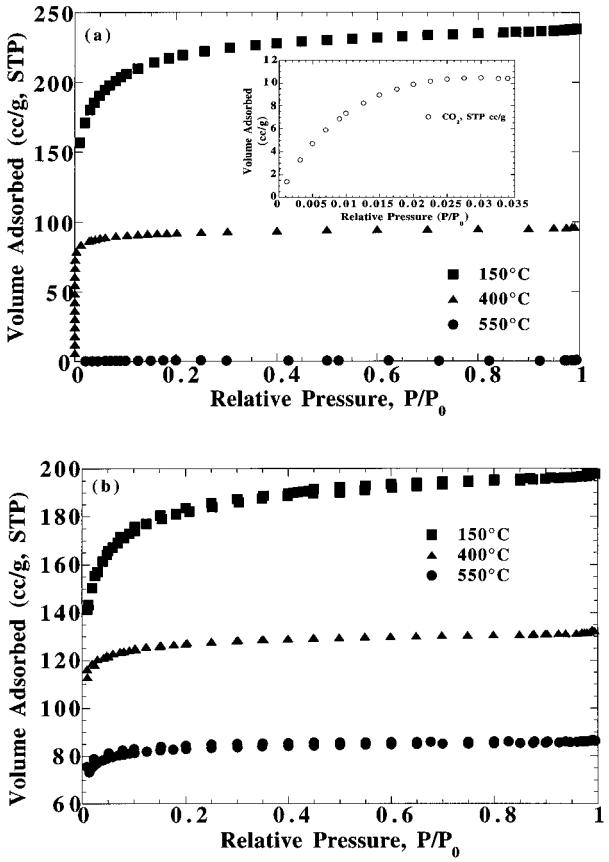

Figure 16. N_2 sorption isotherms of 10 mol % MTES/TEOS (a) and 10 mol % ETES/TEOS (b) xerogels as a function of calcination temperature. Inset shows the partial CO_2 isotherm of the 550 °C calcined MTES/TEOS sample.

Overall many contradictory results emerge from the literature with respect to controlling the microstructure of gels using bridged templates. Corriu et al.[96] observed the pore size and surface area of xerogels prepared with rigid and flexible bridged precursors under acid- and base-catalyzed conditions, was extremely dependent on the reaction conditions, whereas the molecular structure of the template precursor did not lead to large differences in the gel microstructure. The same precursor under identical reaction conditions gave surface areas of 129 or 1262 m^2/g when the catalyst was modified and the surface areas increased from 19 to 685 m^2/g when the solvent was changed from tetrahydrofuran to methanol. In contrast, strong correlation was found by Oviatt et al.[93] between the molecular structure of the template precursor and the gel microstructure. While the porosity and the surface area of the xerogels prepared from bridged templates (phenyl and biphenyl bridged) did not vary appreciably under identical reaction conditions, the surface area and the pore size of the xerogels prepared from flexible templates (alkylene bridged), under both acid- and base-catalyzed conditions, decreased as the length of the alkylene spacer increased beyond C_6. In particular, the surface area of base-catalyzed gels decreased monotonically from 729 to 5 m^2/g as the length of the spacer increased from C_2 to C_{10}. They attributed this decrease, based on the appearance of the monomer peak in ^{29}Si NMR studies,[93] to microphase separation between the siloxane and the aliphatic chains in the gel. It is quite likely that increasing hydrophobicity of the aliphatic chains shielded the attached silyl groups from further condensation pro-

moting phase separation of the siloxane and aliphatic groups. As pointed out by Corriu et al.,[96] in addition to the structure of the precursor, other factors such as the matrix/solvent interactions, nature of the catalyst, and concentration might influence the gel microstructure.

In contrast to bridged ligands, the reduced connectivity (lower K_0) of the network brought about by the incorporation of the pendant ligands generally results in comparatively dense xerogels.[89−91,155] However, the microstructure of the xerogels prepared with pendant ligands appears to depend on RTES concentration, drying rate, and the pore fluid composition. Xerogels[156] and thin[87,157] and thick films[89−91] with a wide variety of microstructures have been synthesized from the MTES/TEOS, ETMS/TMOS, and PTES/TEOS systems, respectively. Increasing the RTES concentration decreases the connectivity of the gel network promoting the capillary stress-induced collapse of the network. For example, Fahrenholtz et al.[126] observed that the surface area of the two-step acid−base catalyzed MTES/TEOS gels dropped dramatically from ∼800 to ∼1 m^2/g when the MTES/TEOS ratio was increased from 0 to 70 mol %. Mechanical strength of the gels measured by three-point bend experiments also was found to decrease in direct proportion to the MTES concentration.[126]

In general, to promote the formation of homogeneous dense xerogels, (1) the network should be made flexible enough to promote shrinkage under the influence of the capillary tension, (2) the network should be dried rapidly to suppress condensation and phase separation, and (3) favorable polymer solvent interactions must be maintained throughout drying to avoid any microphase separation.

2.7. Microstructural Evolution during Heating. To uniquely determine the relationship between the size of the template and the size of the pore created in gels and thin films, the reaction, deposition, and drying conditions must be controlled to provide a dense embedding matrix, so that pores are created only by template removal. As shown in Figure 10d−f, the microstructure established during drying continues to evolve during subsequent heat treatment to pyrolyze the alkoxy and template moieties. There are excellent reviews on structural changes that occur during heating of inorganic gels and thin films.[83] During heating, shrinkage occurs due to continued condensation reactions, structural relaxation, and at sufficiently high temperatures viscous sintering.[87] Shrinkage and structural evolution of organic−inorganic gels on heating is less well understood.

The pyrolysis of organic templates may result in shrinkage due to structural relaxation or viscous sintering depending on the extent of condensation and viscosity of the network over the temperature range in which the organic ligands are pyrolyzed.[87] The nature of the ligand and the processing atmosphere along with the size and microstructure of the gel dictates the pyrolysis temperature. If organics are pyrolyzed at low temperature, there is likely to be an accompanying relaxation of the network due to its lower extent of condensation. Conversely, if pyrolysis occurs at high temperature, the low viscosity of the network combined with the sudden appearence of micropores may result in enhanced viscous sintering.

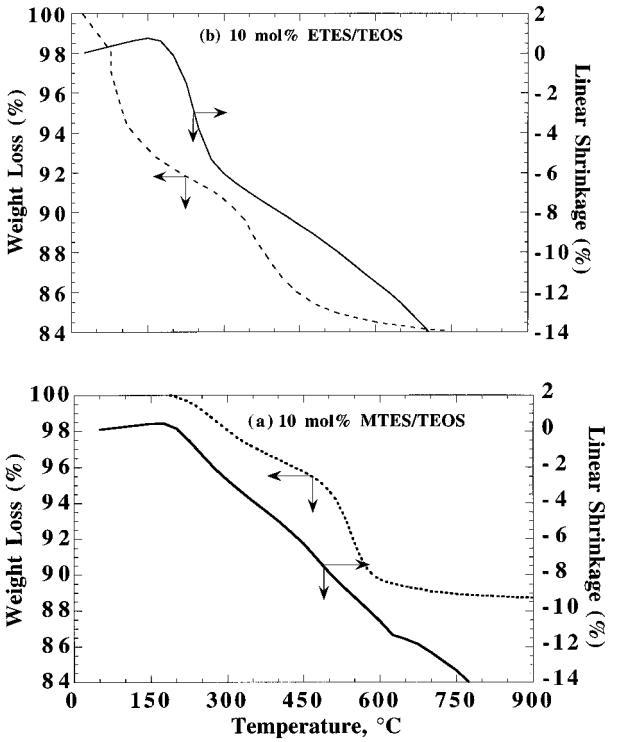

Figure 17. Linear shrinkage and weight loss of the 10 mol % MTES/TEOS (a) and 10 mol % ETES/TEOS (b) xerogels versus temperature. Heating rates of 0.2 and 10 °C/min were used for the linear shrinkage and weight loss experiments, respectively. The higher heating rate displaces the weight loss curve to higher temperatures compared to the shrinkage curve.

Figure 17a,b plots the changes in linear dimension and weight as a function of temperature for 10 mol % MTES/TEOS and 10 mol % ETES/TEOS xerogels which exhibit different behaviors due to their considerably different pyrolysis temperatures. Figure 16a,b shows corresponding N_2 sorption isotherms for samples heated to 150, 400, or 550 °C. Upon heating there is a measurable thermal expansion (30−150 °C) which (based on data for other RTES/TEOS systems) increases with R due to the concomitant reduction in network connectivity.[114,158] Above 200 °C, the MTES/TEOS xerogel shows a monotonic increase in shrinkage. Initially shrinkage is roughly proportional to weight loss suggesting that shrinkage occurs mainly by continued condensation reactions that expel water from the network.[84] Over the range 450−575 °C the gel experiences a sharper weight loss associated with pyrolysis of the methyl groups.[88] There is no corresponding enhancement of shrinkage, indicating that over this temperature range shrinkage does not correlate directly with the removal of organics. The N_2 sorption isotherms show that the initial xerogel is microporous (Type I isotherm). Shrinkage above 150 °C causes a reduction in pore volume and a narrowing of the pore size distribution as evidenced by the much sharper isotherm at 400 °C. By 550 °C the network has densified to the point where there is no measurable N_2 sorption. The corresponding CO_2 isotherm indicates the presence of microporosity.[88] Apparently the high pyrolysis temperature, low connectivity of the network (due to the organic ligands), and creation of microporosity combine to promote viscous sintering by 550 °C, resulting in considerable loss of porosity. It should be noted that due to the constraint imposed by attachment to a substrate, the

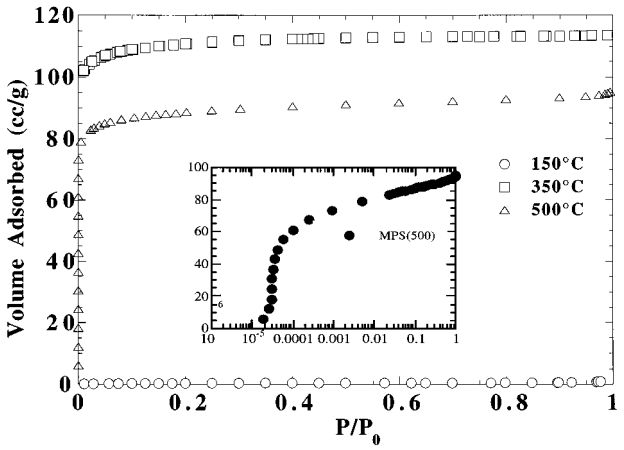

Figure 18. N_2 sorption isotherms of MPS/TEOS (1:4) xerogels as a function of calcination temperature. Inset shows the isotherm at low relative pressure (10^{-6}−1) for the 500 °C heated sample.

sintering of films is retarded compared to bulk specimens, stabilizing the porosity to a higher temperature (see section 2.9).

The ETES/TEOS system shows quite different behavior.[114] Due to the low pyrolysis temperature (200−300 °C), the siloxane network is less condensed (compared to MTES/TEOS) when the organics are removed. The loss of organics causes a commensurate shrinkage, implying that there is little or no porosity created attributable to templating. The corresponding Type I N_2 sorption isotherms (150 and 400 °C) are probably indicative of the original framework porosity. Compared to the MTES/TEOS sample, however, the sample remains microporous at 550 °C, because there is no corresponding enhancement of sintering due to template pyrolysis.

Figure 18 demonstrates a different pathway of microstructure development. The Type II N_2 sorption isotherm obtained after drying[102] is indicative of a denser matrix. Microporosity is clearly created by template pyrolysis at 350 °C and remains to temperatures in excess of 550 °C. Apparently template pyrolysis at intermediate temperatures within a denser matrix (compared to ETES/TEOS) stabilizes the formation of micropores and, due to the lower pyrolysis temperature (compared to MTES/TEOS), does not contribute to enhanced sintering.

2.8. Percolation Threshold. Many applications of sol−gel materials such as adsorbents and membranes require a continuous network of micropores. If the template ligands are randomly distributed in a dense matrix, development of a continuous pore network upon template removal would require that the template volume fraction to exceed a critical value corresponding to a percolation threshold.[159] For an isotropic three-dimensional random network with a coordination number of 12, the site and bond percolation thresholds[130,160,161] occur at ∼20 and ∼12 vol %, respectively. The lower volume fraction seen for bond percolation compared to site percolation arises because of the greater number of nearest neighbors for a bond than for a site.[130]

To date very limited work has been performed to study percolation in organically templated sol−gel silicas. It is inherently difficult to establish a percolation threshold due to the continuing densification of the matrix that alters the porosity of the material during the pyrolysis.[83] However, leaching of phase separated glass[162] in which one phase is preferentially removed does offer some insight about percolation behavior. Shelekhin et al.[132] observed a percolation threshold of 17% for the leachable phase in Vycor glass using Monte Carlo simulations which compares very well with experimental observations.[163,164] For membranes obtained from controlled pyrolysis of polymer fibers, a percolation threshold was reported at 4% and 11% porosity for three-dimensional and two-dimensional randomly oriented fibers, respectively.[134,165] Qualitatively consistent results were obtained by Lu et al.[166] for the percolation threshold in the MPS/TEOS system.

In commonly encountered situations where the embedding matrix is porous at the moment of template pyrolysis and/or the templates are not uniformly dispersed in the matrix (e.g., due to anisotropic shrinkage of films[167,168] or phase separation[119]) continuous porosity may be observed at much lower volume fractions.

2.9. Efficacy of the Template Approach. The overall success of the organic template approach in creating *microporous* silicas can be judged by comparing the pore size and pore volume fractions of the pyrolyzed, extracted, or plasma-treated silicas to the template ligand sizes and concentrations present in the hybrid xerogels.[88,101] These comparisons can be made at least qualitatively on the basis of gas sorption isotherms obtained before and after template removal, e.g., Figures 16 and 18. The Type I isotherms obtained[139] after heating to temperatures just above the pyrolysis temperatures of the methacryloxypropyl (**3**) ligands are indicative of the creation of microporosity (r_p < 1.0 nm) consistent with the template approach. The volumes adsorbed at high relative pressures are a measure of the pore volumes.

Because of their amorphous nature and fine textures, the exact pore sizes of microporous silicas cannot be characterized by conventional techniques such as X-ray diffraction or TEM. Moreover, the determination of average pore size by analyses of Type I sorption isotherms is highly model dependent[169] and biased toward larger pores because of the inaccessability of the smallest pores to the sorbate. Therefore the correspondence between pore size and template size is best established by molecular probe studies[170] using a series of molecules of increasing molecular diameter and measuring a property senstive to adsorption.[171] For example, the permeance of a film (defined as the thickness normalized flux of molecules transported across the film/pressure difference across the film) is sensitive to pore size and volume fraction porosity, and the ratio of the permeances of different gases (referred to as an ideal separation factor) offers a means to establish the pore size.[88]

Relatively few molecular probe studies of this nature have been reported in the literature. Membranes have been prepared from (3-aminopropyl)methyldiethoxysilane (APDS),[172] PTMS/TEOS,[173] MPS/TEOS,[174] and MTES/TEOS.[88] Membranes prepared from APDS were reported to be nonporous, but no study of the effect of removing the organic ligands on pore size or permeance was performed. 25 vol % BESB/TEOS composite films, after pyrolysis of the biphenyl template at 500 °C, exhibited Type II N_2 isotherms (−196 °C) and Type I CO_2

Table 2. Effects of Template Concentration and Calcination Temperature on the Refractive Indexes of Composite Silica/BESB Films Prepared on Silicon Wafers[99] [a]

temp (1 °C/min)	vol % biphenyl templates in silica thin film matrix		
	0%	10%	25%
as-deposited	1.437	1.485	
400 °C	1.419	1.615	2.115
500 °C	1.421	1.388 (~9% porosity)	1.313 (~28% porosity)

[a] Percent porosities were calculated from the refractive index values using Lorentz−Lorenz correlation.[145]

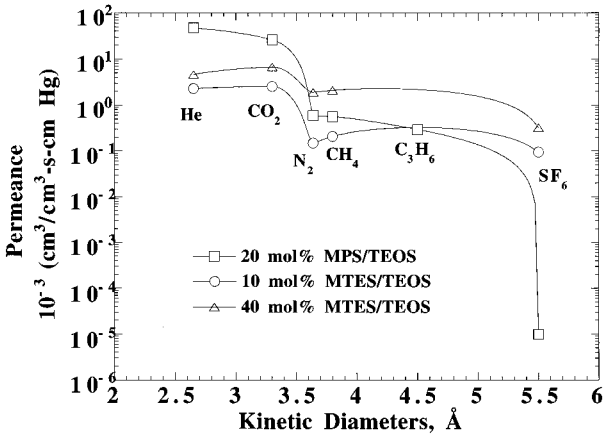

Figure 19. Permeance of the 20 mol % MPS/TEOS and 10 and 40 mol % MTES/TEOS membranes versus the kinetic diameter of gas probe molecules.

isotherms (0 °C) consistent with the formation of ultramicropores (r_p < 0.5 nm). Ellipsometry experiments (Table 2) confirmed that variation of the BESB/TEOS ratio resulted in a commensurate change in porosity.[175] Corresponding membranes[114] showed no molecular discrimination between molecules ranging in diameter from 0.26 to 0.55 nm, qualitatively consistent with expectations based on the estimated size of the biphenyl ligand (~0.87 nm). However, similar results were obtained for membranes prepared from BESP/TEOS, suggesting that the average pore size may be somewhat larger than the estimated size of a bridged phenyl ligand (~0.67 nm).

Cao et al.[144] prepared 20 mol % MPS/TEOS membranes and, after pyrolysis at 300 °C, measured the permeance of a series of five gases, He (0.264 nm), CO_2 (0.33 nm), N_2 (0.364 nm), CH_4 (0.380 nm), and C_3H_6 (0.450 nm). They observed a 44× reduction in membrane permeance in going from CO_2 to N_2 and concluded the average pore diameter to be about 0.35 nm (see Figure 19). This size is considerably smaller than the minimum dimension of a propylene segment (~0.43 nm), indicating that upon pyrolysis there is an accompanying relaxation or consolidation of the silica framework.

Raman et al.[88] performed similar experiments on membranes and thin films prepared from MTES/TEOS hybrid sols. Figure 19 plots permeance versus kinetic diameters of the probe molecules for 10 mol % MTES/TEOS and 40 mol % MTES/TEOS membranes after pyrolysis at 550 °C. Compared to the MPS/TEOS membrane, there is a less abrupt decrease in permeance with increasing probe diameter suggesting a broader size distribution and a larger average pore size.[176] With increasing MTES/TEOS mole ratios the permeance increased consistent with a greater volume fraction porosity.[88]

Raman et al.[113] also used molecular probe techniques to discern the influence of the template ligand size and shape on the resulting pore size. For TEOS, 25 mol % MTES/TEOS and 25 mol % PTMS/TEOS films prepared under identical conditions and pyrolyzed at 550 °C, the radius of the largest alcohol molecule that fit into the pores increased from 0.38 nm (2-propanol) to 0.41 nm (*tert*-butanol) to 0.45 nm (3,5-dimethylbenzyl alcohol), respectively. These data suggest that pore size increases with template size for methyl- and phenyl-templated silicas, but the average pore radius somewhat exceeds the template radii (estimated as ~0.19 nm for methyl and ~0.34 nm for phenyl). This could reflect some adventitious porosity of the network or some incipient phase separation.

With regard to the correspondence between volume fraction template and volume fraction porosity, apart from the data shown in Table 2 for BESB/TEOS films,[99] it is more generally observed that the pore volume fraction is less than that of the templates for molar percentages of organotrialkoxysilanes exceeding about 10%. This appears to stem from relaxation of the network that accompanies template pyrolysis and any enhanced sintering.[84] This effect is more pronounced in systems containing large template concentrations[114] and, especially, for low pyrolysis temperatures due to the lower extents of condensation of the matrix for these situations (see Figure 17b). These effects could be minimized presumably by increasing the extent of condensation of the matrix prior to template pyrolysis.

3. Closing Comments

The mesoporous and microporous silica systems discussed in this paper are representative of two fundamentally different approaches to template-mediated synthesis and processing of porous media. For the case of surfactant-templated mesoporous silica, the organic and inorganic precursor organize cooperatively (but independently) according to strong noncovalent interactions such as electrostatic, hydrogen-bonding, and van der Waals contacts that afford a precise molding of the network around the surfactant assembly. Diverse reaction conditions and reagents usually result in the same mesophase structure, implying the formation of a thermodynamically stable structure. For the case of ligand-templated microporous silicas, the covalently bound template alters the chemical reactivity of the inorganic precursor and confers hydrophobicity to an otherwise hydrophilic network. At each successive stage of the sol−gel process, kinetic control must be employed to avoid phase separation and to "freeze-in" a homogeneous structure. The pathway of structural evolution depends critically upon the preceding synthesis and processing history. Only under a limited set of conditions, that depend strongly on framework−solvent−template interactions and pyrolysis behavior, do we observe a templating effect.

With regard to future prospects, many challenges exist in the field of surfactant-templated materials. Obviously there are many more oxide and non-oxide frameworks that can form mesophases. The key here is to develop methods to efficiently remove the templates

without sacrificing porosity or pore regularity. Other structure types may exist especially in more complex systems, perhaps with more than one type of surfactant. Also, it would be advantageous to have crystalline frameworks for some catalytic applications. Crack-free continuous membranes would be appropriate for separations applications. Finally, a better understanding of how to control porosity must emerge so that materials can be custom tailored to suit applications.

The difficulty in characterizing the microstructure and the relatively large number of processing variables, in the case of covalently bonded templates, makes it harder to establish a direct correlation between the size of the template and the pore size created. More information is needed regarding the nature and strength of nonbonded interactions between the template, the framework, and the solvents that ultimately determine the efficacy of the template approach. New characterization techniques should be developed to better understand phase separation and microstructural evolution during heating. The use of more hydrophilic templating ligands must be explored in more detail along with the use of bridging ligands as micropore templates. Finally, low-temperature extraction procedures should be more thoroughly explored to avoid structural relaxation and sintering.

The two classes of templates discussed in this paper, namely, noncovalently and covalently bonded templates, represent the two bounds of nanostructured materials with respect to structure direction—thermodynamic and kinetic. In surfactant-templated materials, diverse reaction conditions and reagents usually result in the same mesophase structure, implying the formation of a thermodynamically metastable structure, whereas in the covalently bonded template materials the reaction conditions and precursors dictate the kinetic pathway, leading to vastly different final microstructures. Also, the larger size and weaker interactions of the surfactant templates increase the selectivity of the templates to form specific mesophases with little structural rearrangements, whereas the smaller size and strong covalent bonding cause extensive structural rearrangements to occur during processing, reducing the registration between the template size and the pore size created. The results presented in this review constitute only a fraction of the numerous possibilities that exist with respect to the size of the templates and processing conditions that can be used to synthesize nanostructured materials. Obviously, a better understanding of the processing−structure−property relationships in these systems would help in the rational synthesis of porous materials.

Acknowledgment. Portions of this work were supported by the Electric Power Research Institute, the National Science Foundation (CTS 9101658), the Gas Research Institute, and the Department of Energy—Morgantown Energy Technology Center, and Basic Energy Sciences Program. M.T.A. wishes to acknowledge Dr. J. E. Martin of Sandia National Laboratories (SNL) for a fruitful collaboration. In addition, we are grateful to Dr. J. Samuel of SNL for providing results of thin-film stress measurements and to Dr. D. A. Loy of SNL for providing useful discussions of hybrid sol−gel chemistry and processing. Dr. G. Cao and Mr. Y.-F. Lu of University of New Mexico are also acknowledged for providing unpublished results concerning the MPS/TEOS system. SNL is a United States Department of Energy facility operated under Contract No. DE-AC04-94AL85000.

References

(1) Schaefer, D. W. *MRS Bull.* **1994**, *19*, 14.
(2) Davis, M. E. *Nature* **1993**, *364*, 391.
(3) Behrens, P. *Adv. Mater.* **1993**, *5*, 127.
(4) Ozin, G. A.; Gil, C. *Chem. Rev.* **1989**, *89*, 1749.
(5) Herron, N. In: *Inclusion Compounds*; Atwood, J. L., Davis, J. E. D., MacNicol, D. D., Eds.; Oxford University Press: Oxford, 1991; Vol. 5, p 90.
(6) Stucky, G. D.; MacDougall, J. E. *Science* **1990**, *247*, 669.
(7) Zhang, Y.; Raman, N. K.; Bailey, J. K.; Brinker, C. J.; Crooks, R. M. *J. Phys. Chem.* **1992**, *96*, 9098.
(8) Cox, S. D.; Gier, T. E.; Stucky, G. D. *Chem. Mater.* **1990**, *2*, 609.
(9) Bein, T.; Enzel, P. *Angew. Chem., Int. Ed. Engl.* **1989**, *28*, 1692.
(10) Pauling, L.; Campbell, D. H. *J. Exptl. Med.* **1942**, *76*, 211.
(11) Dickey, F. H. *Proc. Natl. Acad. Sci. U.S.A.* **1949**, *35*, 227.
(12) Beck, J. S.; Vartuli, J. C.; Kennedy, G. J.; Kresge, C. T.; Roth, W. J.; Schramm, S. E. *Chem. Mater.* **1994**, *6*, 1816.
(13) Wulff, G.; Sarhan, A.; Zabrocki, K. *Tetrahedron Lett.* **1973**, 4329.
(14) Andersson, L.; Sellergren, B.; Mosbach, K. *Tetrahedron Lett.* **1984**, *25*, 5211.
(15) Sellergren, B. *Chirality* **1989**, *1*, 63.
(16) Burkett, S. L.; Davis, M. E. *Chem. Mater.* **1995**, *7*, 920.
(17) Burkett, S. L.; Davis, M. E. *Chem. Mater.* **1995**, *7*, 1453.
(18) Kresge, C. T.; Leonowicz, M. E.; Roth, W. J.; Vartuli, J. C.; Beck, J. S. *Nature* **1992**, *359*, 710.
(19) Stucky, G. D.; Monnier, A.; Schuth, F.; Huo, Q.; Margolese, D.; Kumar, D.; Krishnamurty, M.; Petroff, P.; Firouzi, A.; Janicke, M.; Chmelka, B. F. *Mol. Cryst. Liq. Cryst.* **1994**, *240*, 187.
(20) Heilmann, J.; Maier, W. F. *Angew. Chem., Int. Ed. Engl.* **1994**, *33*, 471.
(21) Lawton, S. L.; Rohrbaugh, W. J. *Science* **1990**, *247*, 1319.
(22) (a) Breck, D. W. *Zeolite Molecular Sieves*; Robert E. Kreiger Publishers: Florida, 1984; p 639. (b) Barrer, R. M. *Hydrothermal Synthesis of Zeolites*; Academic: London, 1982.
(23) Beck, J. S.; Vartuli, J. C.; Roth, W. J.; Leonowicz, M. E.; Kresge, C. T.; Schmitt, K. D.; Chu, C. T.-W.; Olson, K. H.; Sheppard, E. W.; McCullen, S. B.; Higgins, J. B.; Schlenker, J. L. *J. Am. Chem. Soc.* **1992**, *114*, 10834−10843.
(24) Beck, J. S.; Vartuli, J. C. *Curr. Opinion Solid State Mater. Sci.* **1996**, *1*, 76−87.
(25) Behrens, P. *Angew. Chem., Int. Ed. Eng.* **1996**, *35*(5), 515−518.
(26) Davis, M. E.; Lobo, R. F. *Chem. Mater.* **1992**, *4*, 756.
(27) Lobo, R. F.; Zones, S. I.; Davis, M. E. *J. Inc. Phen. Mol. Rec. Chem.* **1995**, *21*, 47−78.
(28) Monnier, A.; Schuth, F.; Huo, Q.; Kumar, D.; Margolese, D. I.; Maxwell, R. S.; Stucky, G. D.; Krishnamurty, M.; Petroff, P.; Firouzi, A.; Janicke, M.; Chmelka, B. F. *Science* **1993**, *261*, 1299−1303.
(29) Tanev, P. T.; Pinnavaia, T. J. *Science* **1995**, *267*, 865−867.
(30) Kloetstra, K. R.; van Bekkum, H. J. *Chem. Res., Synop.* **1995**, *1*, 26−27.
(31) Armengol, E.; Maria, L.; Corma, A.; Garcia, G.; Navarro, M. T. *J. Chem. Soc., Chem. Commun.* **1995**, *5*, 519−520.
(32) Kloetstra, K. R.; van Bekkum, H. *J. Chem. Soc., Chem. Commun.* **1995**, *10*, 1005−1006.
(33) Corma, A.; Fornes, V.; Navarro, M. T.; Perez-Pariente, J. *J. Catal.* **1994**, *148*, 569.
(34) Chen, C.-Y.; Li, H.-X.; Davis, M. E. *Micropor. Mater.* **1993**, *2*, 17−26.
(35) Corma, A.; Navarro, M. T.; Perez-Pariente, P. *J. Chem. Soc., Chem. Commun.* **1994**, 147.
(36) Tanev, P. T.; Chibwe, M.; Pinnavaia, T. J. *Nature* **1994**, *368*, 321.
(37) Schuth, F. *Ber. Bunsen.-Ges. Phys. Chem.* **1995**, *99*, 1306−1315.
(38) Armengol, E.; Cano, M. L.; Corma, A.; Garcia, H.; Navarro, M. T. *J. Chem. Soc., Chem. Commun.* **1995**, 519−520.
(39) Llewellyn, P. L.; Ciesla, U.; Decher, H.; Stadler, R.; Schüth, F.; Ünger, K. in *Zeolites and Related Microporous Materials: State of the Art 1994, Stud. in Surf. Sci. and Catal. Proceedings of the 10th International Zeolite Conference Garmisch-Partenkirchen Germany*; Weitkamp, J., Karge, J. G., Pfeifer, J., Holderich, W., Eds.; Elsevier: Amsterdam, 1994; Vol. 84, p 2013.
(40) Corma, A.; Martinez, A.; Martinez-Soria, V.; Monton, J. B. *J. Catal.* **1995**, *153*, 25.
(41) Kresge, C. T.; Marler, D. O.; Rav, G. S.; Rose, B. H. U.S. Patent 5,366,945, 1994.
(42) Kozhevnikov, I. V.; Sinnema, A.; Jansen, R. J. J.; Pamin, K.; van Bekkum, H. *Catal. Lett.* **1995**, *30*, 241−252.
(43) Maschmeyer, T.; Rey, F.; Sankar, G.; Thomas, J. M. *Nature* **1995**, *378*, 159−161.

(44) Wu, C.-G.; Bien, T. *Science* **1994**, *264*, 1757−1759.
(45) Wu, C.-G.; Bien, T. *Science* **1994**, *266*, 1013.
(46) Huber, C.; Moller, K.; Bein, T. J. *J. Chem. Soc., Chem. Commun.* **1994**, 2619−2620.
(47) Corma, A.; Fornes, V.; Garcia, H.; Miranda, M. A.; Sabater, M. J. *J. Am. Chem. Soc.* **1994**, *116*, 9767−9768.
(48) Olson, D. H.; Stucky, G. D.; Vartuli, J. C. U.S. Patent 5,364,797, 1994.
(49) Martin, J. E.; Anderson, M. T.; Odenik, J.; Newcomer, P. *Langmuir*, submitted.
(50) For overviews of surfactants see: (a) Rosen, M. J. *Surfactants and Interfacial Phenomena*, 2nd ed.; Wiley: New York, 1989. (b) Myers, D. *Surfactant Science and Technology*, 2nd ed.; VCH: New York, 1992.
(51) Israelachvili, J. N.; Mitchell, D. J.; Ninham, B. W. *J. Chem. Soc., Faraday Trans. 2* **1976**, *72*, 1527.
(52) Huo, Q.; Margolese, D. I.; Ciesla, U.; Demuth, D. G.; Feng, P.; Gier, T. E.; Sieger, P.; Firouzi, A.; Chmelka, B. F.; Schuth, F.; Stucky, G. D. *Chem. Mater.* **1994**, *6*, 1176−1191.
(53) Antonelli, D. M.; Ying, J. Y. *Angew. Chem., Int. Ed. Engl.* **1995**, *34*, 2014−2017.
(54) Bagshaw, S. A.; Prouzet, E.; Pinnavaia, T. J. *Science* **1995**, *269*, 1242−1244.
(55) Attard, G. S.; Glyde, J. C.; Goltner, C. G. *Nature* **1995**, *378*, 366−368.
(56) Anderson, M. T.; Martin, J. E.; Odinek, J.; Newcomer, P., submitted to *Chem. Mater.*
(57) Luan, Z.; Cheng, C.-F.; Zhou, W.; Klinowski, J. *J. Phys. Chem.* **1995**, *99*, 1018−1024.
(58) Borade, R. B.; Clearfield, A. *Catal. Lett.* **1995**, *31*, 267−272.
(59) Luan, Z.; He, H.; Zhou, W.; Cheng, C-F.; Klinowski, J. *J. Chem. Soc., Faraday Trans.* **1995**, *91*, 2955−2959.
(60) Reddy, K. M.; Moudrakovski, I.; Sayari, A. *J. Chem. Soc., Chem. Commun.* **1994**, 1059.
(61) Sayari, A.; Danumah, C.; Moudrakovski, I. L. *Chem. Mater.* **1995**, *7*, 813−815.
(62) Yuan, Z. Y.; Liu, S. Q.; Chen, T. H.; Wang, J. Z.; Li, H. X. *J. Chem. Soc., Chem. Commun.* **1995**, *9*, 973−974.
(63) Zhao, D.; Goldfarb, D. *J. Chem. Soc., Chem. Commun.* **1995**, *8*, 875−976.
(64) Cheng, C.-F.; He, H.; Zhou, W.; Klinowski, J.; Goncalves, J. A. S.; Gladden, L. F. *J. Phys Chem.* **1996**, *100*, 390−396.
(65) Ciesla, U.; Schacht, S.; Stucky, G. D.; Unger, K. K.; Schuth, F. *Angew. Chem., Int. Ed. Engl.* **1996**, *35*, 541−543.
(66) Luca, V.; MacLachlan, D. J.; Hook, J. M.; Withers, R. *Chem. Mater.* **1995**, *7*, 2220−2223.
(67) Abe, T.; Taguchi, A.; Iwamoto, M. *Chem. Mater.* **1995**, *7*, 1429−1430.
(68) Antonelli, D. M.; Ying, J. Y. *Chem. Mater.* **1996**, *8*, 874−881.
(69) Anderson, M. T.; Newcomer, P. *Mater. Res. Soc. Symp. Proc.* **1995**, *371*, 117−121.
(70) Ozin, et al. *Supramolecular Chemistry: Proceedings of the Molecular Recognition Conference*; Ottawa, May, 1994.
(71) Huo, Q.; Margolese, D. I.; Ciesla, U.; Feng, P.; Gier, T. E.; Sieger, P.; Leon, R.; Petroff, P. M.; Schuth, F.; Stucky, G. D. *Nature* **1994**, *24*, 317−321.
(72) Chen, C.-Y.; Burkett, S. L.; Li, H.-X.; Davis, M. E. *Micropor. Mater.* **1993**, *2*, 27−34.
(73) Vartuli, J. C.; Kresge, C. T.; Leonowicz, M. E.; Chu, A. S.; McCullen, S. B.; Johnson, I. D.; Sheppard, E. W. *Chem. Mater.* **1994**, *6*, 2070−2077.
(74) Steel, A.; Carr, S. W.; Anderson, M. W. *J. Chem. Soc., Chem. Commun.* **1994**, 1571.
(75) Firouzi, A.; Kumar, D.; Bull, L. M.; Besier, T.; Sieger, P.; Huo, Q.; Walker, S. A.; Zasadzinski, J. A.; Glinka, C.; Nicol, J.; Margolese, D.; Stucky, G. D.; Chmelka, B. F. *Science* **1995**, *267*, 1138−1143.
(76) Quirion, F.; Magid, L. J. *J. Phys. Chem.* **1986**, *90*, 5435.
(77) Gamboa, C.; Rios, H.; Sepulveda, L. *J. Phys. Chem.* **1989**, *93*, 5540.
(78) Lindemuth, P. M.; Bertrand, G. *J. Phys. Chem.* **1993**, *97*, 7769.
(79) Backlund, S.; Hoiland, H.; Kvammen, O. J.; Ljosland, E. *Acta Chem. Scand.* **1982**, *A36*, 698.
(80) Ozeki, S.; Ikeda, S. *Bull. Chem. Soc. Jpn.* **1981**, *54*, 552.
(81) Ideda, S. *Colloid Polym. Sci.* **1991**, *269*, 49.
(82) Fyfe, C. A.; Fu, G. *J. Am. Chem. Soc.* **1995**, *117*, 9709−9714.
(83) As determined by peak width broadening in X-ray diffraction experiments, also the number of peaks in the diffraction pattern.
(84) Klevens, H. B. *J. Phys. Colloid Chem.* **1948**, *52*, 130.
(85) Czerniawski, M. *Roczn. Chem.* **1966**, *40*, 1935.
(86) It is important to note that MCM-41-type materials do not exhibit Bragg reflections from planes parallel to their tubes (i.e., in *hkl*, $l = 0$), and thus long-range order simply refers to the regularity of the honecomb network of pores. For applications in which transport in to and out of the materials is critical, the regularity along the direction of the pores is probably far more important. Unfortunately, this is quite difficult to routinely analyze.
(87) Cheng, C.-F.; Luan, Z.; Klinowski, J. *Langmuir* **1995**, *11*, 2815−2819.
(88) Yanagisawa, T.; Shimizu, T.; Kuroda, K.; Kato, C. *Bull. Chem. Soc. Jpn.* **1990**, *63*, 988.
(89) Inagaki, S.; Fukushima, Y.; Kuroda, K. *J. Chem. Soc., Chem. Commun.* **1993**, 680−682.
(90) Chen, C.-Y.; Xiao, S. Q.; Davis, M. E. *Micropor. Mater.* **1995**, *4*, 1.
(91) Vartuli, J. C.; Kresge, C. T.; Leonowicz, M. E.; Chu, A. S.; McCullen, S. B.; Johnson, I. D.; Sheppard, E. W. *Chem. Mater.* **1994**, *6*, 2070−2077.
(92) Inagaki, S.; Fukushima, Y.; Kuroda, K. In *Proceedings: Symposium on Synthesis of Zeolites, Layered Compounds and Other Microporous Solids: 209th National Meeting*; April 2−7, 1995; American Chemical Society, Anaheim, CA.
(93) Branton, P. J.; Hall, P. G.; Sing, K. S. W.; Reicher, J.; Schuth, F.; Unger, K. K. *J. Chem. Soc., Faraday Trans.* **1994**, *90*, 2965−2967.
(94) Branton, P. J.; Hall, P. G.; Sing, K. S. W. *J. Chem. Soc., Chem. Commun.* **1993**, 1257−1258.
(95) Llewellyn, P. L.; Grillet, Y.; Schuth, F.; Reichert, J.; Unger, K. K. *Micropor. Mater.* **1994**, *3*, 345−349.
(96) Branton, P. J.; Hall, P. G.; Treguer, M.; Sing, K. S. W. *J. Chem. Soc., Faraday Trans.* **1995**, *91*, 2041−2043.
(97) Rathousky, J.; Zukal, A.; Franke, O.; Schulz-Ekloff, G. *J. Chem. Soc., Faraday Trans.* **1995**, *91*, 937−940.
(98) Beck, J. S.; Calabro, D. C.; McCullen, ; Pelrine, B. P.; Schmitt, K. D.; Vartuli, J. C. U.S. Patent 5,145,816, 1992.
(99) Beck, J. S. U.S. Patent 5,057,296, 1991.
(100) Kushalani, K.; Kuperman, A.; Ozin, G. A.; Tanaka, K.; Garces, J.; Olken, M. M.; Coombs, N. *Adv. Mater.* **1995**, *7*, 842−846.
(101) Anderson, M. T.; Martin, J. E.; Odinek, J.; Newcomer, P., to be submitted to *Chem. Mater.*
(102) Kim, J. M.; Kwak, J. H.; Jun, S.; Ryoo, R. *J. Phys. Chem.* **1995**, *99*, 16742−16747.
(103) Ryoo, R.; Kim J. M *J. Chem. Soc., Chem. Commun.* **1995**, 711−712.
(104) Morey, M.; Davidson, A.; Eckert, H.; Stucky, G. *Chem. Mater.* **1996**, *8*, 486−492.
(105) Lin, W.; Sun, Y.; Pang, W. *J. Chem. Soc., Chem. Commun.* **1995**, 2367.
(106) Anderson, M. T.; Martin, J. E.; Odinek, J.; Newcomer, P., to be submitted to *Micropor. Mater.*
(107) Ogawa, M. *J. Am. Chem. Soc.* **1994**, *116*, 7941−7942.
(108) Yang, H.; Kuperman, A.; Coombs, N.; Mamiche-afara, S.; Ozin, G. A. *Nature* **1996**, *379*, 703−705.
(109) Bontha, J. R.; Kim, A. Y.; Liu, J. *Mater. Res. Soc. Symp. Proc. P: Microporous and Macroporous Materials*; April 8−12, San Francisco, CA, 1996.
(110) IUPAC classifies porous materials based on their pore diameters, *d*: (1) microporous—$d < 20$ Å, (2) mesoporous—$20 \leq d \leq 500$ Å, and (3) macroporous—$d > 500$ Å.
(111) Brinker, C. J.; Raman, N. K.; Logan, M. N.; Sehgal, R.; Assink, R. A.; Hua, D.-W.; Ward, T. L. *J. Sol-Gel Sci. Technol.* **1995**, *4*, 117.
(112) Brinker, C. J.; Scherer, G. W. *Sol-Gel Science: The Physics and Chemistry of Sol-Gel Processing*; Academic Press: San Diego, CA, 1990.
(113) Brinker, C. J.; Ward, T. L.; Sehgal, R.; Raman, N. K.; Hietala, S. L.; Smith, D. M.; Hua, D.-W.; Headley, T. J. *J. Membr. Sci.* **1993**, *77*, 165.
(114) Sehgal, R.; Brinker, C. J. *Supported Inorganic Membranes*, U.S. Patent Application, filed Nov 1995.
(115) Raman, N. K.; Ward, T. L.; Brinker, C. J.; Sehgal, R.; Smith, D. M.; Duan, Z.; Hampden-Smith, M.; Bailey, J. K.; Headley, T. *Appl. Cat.* **1993**, *69*, 65.
(116) Raman, N. K.; Brinker, C. J. *J. Membr. Sci.* **1995**, *105*, 273.
(117) Sanchez, C.; Ribot, F. *First European Workshop on Hybrid Organic-Inorganic Materials:* Sanchez, C., Ribot, F., Eds.; Paris, 1993; p 9.
(118) Schmidt, H.; Seiferling, B. *Mater. Res. Soc. Symp. Proc.* **1986**, *73*, 739.
(119) Schmidt, H.; Rinn, G.; Nab, R.; Sporn, D. *Mater. Res. Soc. Symp. Proc.* **1988**, *121*, 743.
(120) Schmidt, H.; Wolter, H. *J. Non-Cryst. Solids* **1990**, *121*, 428.
(121) Liu, C.; Komarneni, S. *Mater. Res. Soc. Symp. Proc.* **1995**, *371*, 217.
(122) Oviatt, H. W.; Shea, K. J.; Small, J. H. *Chem. Mater.* **1993**, *5*, 943.
(123) Loy, D. A.; Shea, K. J.; Buss, R. J.; Assink, R. A. *ACS Symp. Ser.* **1994**, *572*, 122.
(124) Loy, D. A.; Buss, R. J.; Assink, R. A.; Shea, K. J.; Oviatt, H. *Mater. Res. Soc. Symp. Proc.* **1994**, *346*, 825.
(125) Corriu, R. J. P.; Moreau, J. J. E.; Thepot, P.; Chi Man, M. W. *Chem. Mater.* **1992**, *4*, 1217.
(126) Delattre, L.; Dupuy, C.; Babonneau, F. *First European Workshop on Hybrid Organic-Inorganic Materials*; Sanchez, C., Ribot, F., Eds.; Paris, 1993; p 185.
(127) Brinker, C. J.; Sehgal, R.; Hietala, S. L.; Deshpande, R.; Smith, D. M.; Loy, D.; Ashley, C. S. *J. Membr. Sci.* **1994**, *94*, 85.
(128) Coleman, M. M.; Serman, C. J.; Bhagwagar, D. E.; Painter, P. C. *Polym. Rev.* **1990**, *31*, 1187.

(129) Olabisi, O.; Robeson, L. M.; Shaw, M. T. *Polymer-Polymer Miscibility*; Academic Press: New York, 1979; Chapter 4.
(130) Li, X.; King, T. A. *Mater. Res. Soc. Symp. Proc.* **1994**, *346*, 541.
(131) Raman, N. K.; Brinker, C. J.; Delattre, L.; Prakash, S. S. *Proc. ICIM[3'94]*; Ma, Y. H., Ed.; *Third International Conference on Inorganic Membranes*; Worcester, MA, 1994; p 63.
(132) Prabakar, S.; Assink, R. A.; Raman, N. K.; Myers, S. A.; Brinker, C. J. *J. Non-Cryst. Solids*, in press.
(133) Kaji, H.; Nakanishi, K.; Soga, N. *J. Non-Cryst. Solids* **1995**, *181*, 16.
(134) Coltrain, B. K.; Landry, C. J. T.; O'Reilly, J. M.; Chamberlain, A. M.; Rakes, G. A.; Sedite, J. S.; Kelts, L. W.; Landry, M. R.; Long, V. K. *Chem. Mater.* **1993**, *5*, 1445.
(135) Chambers, R. C.; Jones, W. E.; Haruvy, Y.; Webber, S. E.; Fox, M. A. *Chem. Mater.* **1993**, *5*, 1481.
(136) Smaihi, M.; Jermoumi, T.; Marignan, J. *Chem. Mater.* **1995**, *7*, 2293.
(137) Fyfe, C. A.; Zhang, Y.; Aroca, P. *J. Am. Chem. Soc.* **1992**, *114*, 3252.
(138) van Bommel, M. J.; Bernards, T. N. M.; Boonstra, A. H. *J. Non-Cryst. Solids* **1991**, *128*, 231.
(139) Capozzi, C. A.; Pye, L. D.; Condrate Sr., R. A. *Mater. Lett.* **1992**, *15*, 130.
(140) McNeil, K. J.; Dicarpio, J. A.; Walsh, D. A.; Pratt, R. F. J. *J. Am. Chem. Soc.* **1980**, *102*, 1859.
(141) Sugahara, Y.; Okada, S.; Sato, S.; Kuroda, K.; Kato, C. *J. Non-Cryst. Solids* **1994**, *167*, 21.
(142) Sakka, S.; Tanaka, Y.; Kokubo, T. *J. Non-Cryst. Solids* **1986**, *82*, 24.
(143) Raman, N. K.; Brinker, C. J. Unpublished results.
(144) Stauffer, D.; Coniglio, A.; Adam, M. *Adv. Polym. Sci.* **1982**, *44*, 105.
(145) Schaefer, D. W.; Bunker, B. C.; Wilcoxon, J. P. In *Fractals in the Natural Sciences*; Fleishmann, M., Tildesley, D. J., Ball, R. C., Eds.; 1989; p 35.
(146) Scherer, G. W. *Mater. Res. Soc. Symp. Proc.* **1988**, *121*, 179.
(147) Tanaka, T. *Sci. Am.* **1981**, *244*, 124.
(148) Quinson, J. F.; Tchipkam, N.; Dumas, J.; Bovier, C.; Serughetti, J.; Guizard, C.; Larbot, A.; Cot, L. *J. Non-Cryst. Solids* **1988**, *99*, 151.
(149) Raman, N. K.; Wallace, S.; Brinker, C. J. *J. Non-Cryst. Solids*, in press.
(150) Moore, F. *Trans. Brit. Ceram. Soc.* **1961**, *60*, 517.
(151) Banks, W. H.; Barkas, W. W. *Nature* **1946**, *158*, 341.
(152) Smith, D. M.; Scherer, G. W.; Anderson, J. M. *J. Non-Cryst. Solids*, in press.
(153) deGennes, P. G. *Scaling Concepts in Polymer Physics*; Cornell University Press: New York, 1991.
(154) Polevaya, Y.; Samuel, J.; Ottolenghi, M.; Avnir, D. *J. Sol-Gel Sci. Technol.* **1995**, *5*, 65.
(155) Cao, G.; Lu, Y.; Delattre, L.; Brinker, C. J.; Lopez, G. P. *Adv. Mater.*, in press.
(156) Fahrenholtz, W. G.; Smith, D. M.; Hua, D.-W. *J. Non-Cryst. Solids* **1992**, *144*, 45.
(157) Haruvy, Y.; Webber, S. E. *Chem. Mater.* **1992**, *4*, 89.
(158) Innocenzi, P.; Abdirashid, M. O.; Guglielmi, M. *J. Sol-Gel Sci. Technol.* **1994**, *3*, 47.
(159) Zallen, R. *The Physics of Amorphous Solids*; Wiley-Interscience: New York, 1983.
(160) Sahimi, M.; Gavalas, G. R.; Tsotsis, T. T. *Chem. Eng. Sci.* **1990**, *45*, 1443.
(161) A random porous media can be represented by a discrete model in which the pore space exists as a network of bonds and sites: see p 1469 in ref 131.
(162) Shelekhin, A. B.; Dixon, A. G.; Ma, Y. H. *J. Membr. Sci.* **1993**, *83*, 181.
(163) Shelekhin, A. B.; Grosgogeat, E. J.; Hwang, S. T. *J. Membr. Sci.* **1991**, *66*, 129.
(164) Tomadakis, M. M.; Sotirchos, S. V. *AICHE J.* **1991**, *37*, 1175.
(165) Tomadakis, M. M.; Sotirchos, S. V. *AICHE J.* **1991**, *37*, 74.
(166) Lu, Y.; Brinker, C. J., unpublished results.
(167) Garino, T. J. *Mater. Res. Soc. Symp. Proc.* **1990**, *180*, 497.
(168) Garino, T. J.; Bowen, H. K. *J. Am. Ceram. Soc.* **1990**, *73*, 251.
(169) Gregg, S. J.; Sing, K. S. W. *Adsorption, Surface Area, and Porosity*; Academic Press: New York, 1982; p 209.
(170) Voncken, J. H. L.; Lijzenga, C.; Kumar, K. P.; Keizer, K.; Burggraaf, A. J.; Bonekamp, B. C. *J. Mater. Sci.* **1992**, *27*, 472.
(171) Samuel, J.; Brinker, C. J.; Hurd, A. J.; Cairncross, R. A.; Yan, H.; Niemczyk, T. M. *Nature*, submitted.
(172) Guizard, C.; Lacan, P. First European Workshop on Hybrid Organic-Inorganic Materials; Sanchez, C., Ribot, F., Eds.; Paris, 1993; p 153.
(173) Okui, T.; Saito, Y.; Okubo, T.; Sadakata, M. *J. Sol-Gel Sci. Technol.* **1995**, *5*, 127.
(174) Cao, G.; Lu, Y.; Delattre, L.; Brinker, C. J.; Lopez, G. P. *Adv. Mater.*, in press.
(175) Tompkins, H. G. *A User's Guide To Ellipsometry*; Academic Press: San Diego, CA, 1993.
(176) The constraint to sintering imposed by the substrate stabilizes the microporosity to higher temperatures in the thin film/membrane samples.

CM960138+